


Tracing Isomanifolds in \mathbb{R}^d in Time Polynomial in d using Coxeter-Freudenthal-Kuhn Triangulations

Jean-Daniel Boissonnat 

Université Côte d'Azur, Inria
[Sophia-Antipolis, France]

Sargey Kachanovich 

Université Côte d'Azur, Inria
[Sophia-Antipolis, France]

Mathijs Wintraecken  

IST Austria
[Klosterneuburg, Austria]

1 — Abstract —

2 Isomanifolds are the generalization of isosurfaces to arbitrary dimension and codimension, i.e.
3 submanifolds of \mathbb{R}^d defined as the zero set of some multivariate multivalued smooth function
4 $f: \mathbb{R}^d \rightarrow \mathbb{R}^{d-n}$, where n is the intrinsic dimension of the manifold. A natural way to approximate
5 a smooth isomanifold \mathcal{M} is to consider its Piecewise-Linear (PL) approximation $\hat{\mathcal{M}}$ based on a
6 triangulation \mathcal{T} of the ambient space \mathbb{R}^d . In this paper, we describe a simple algorithm to trace
7 isomanifolds from a given starting point. The algorithm works for arbitrary dimensions n and d , and
8 any precision D . Our main result is that, when f (or \mathcal{M}) has bounded complexity, the complexity
9 of the algorithm is polynomial in d and $\delta = 1/D$ (and unavoidably exponential in n). Since it is
10 known that for $\delta = \Omega(d^{2.5})$, $\hat{\mathcal{M}}$ is $O(D^2)$ -close and isotopic to \mathcal{M} , our algorithm produces a faithful
11 PL-approximation of isomanifolds of bounded complexity in time polynomial in d . Combining this
12 algorithm with dimensionality reduction techniques, the dependency on d in the size of $\hat{\mathcal{M}}$ can be
13 completely removed with high probability. We also show that the algorithm can handle isomanifolds
14 with boundary and, more generally, isostratifolds. The algorithm for isomanifolds with boundary
15 has been implemented and experimental results are reported, showing that it is practical and can
16 handle cases that are far ahead of the state-of-the-art.

2012 ACM Subject Classification Theory of computation \rightarrow Computational geometry

Keywords and phrases Coxeter triangulation, Kuhn triangulation, permutahedron, PL-approximations, isomanifolds/solution manifolds/isosurfacing

Related Version A full version of this paper is available at <https://hal.archives-ouvertes.fr/hal->

Funding The research leading to these results has received funding from the European Research Council (ERC) under the European Union's Seventh Framework Programme (FP/2007-2013) / ERC Grant Agreement No. 339025 GUDHI (Algorithmic Foundations of Geometry Understanding in Higher Dimensions).

Jean-Daniel Boissonnat: Supported by the French government, through the 3IA Côte d'Azur Investments in the Future project managed by the National Research Agency (ANR) with the reference number ANR-19-P3IA-0002.

Mathijs Wintraecken: Supported by the European Union's Horizon 2020 research and innovation programme under the Marie Skłodowska-Curie grant agreement No. 754411.

Acknowledgements We thank Dominique Attali, Guilherme de Fonseca, Arijit Ghosh, Vincent Pilaud and Aurélien Alvarez for their comments and suggestions. We also acknowledge the reviewers.



© Jean-Daniel Boissonnat, Sargey Kachanovich, and Mathijs Wintraecken;
licensed under Creative Commons License CC-BY 4.0

37th International Symposium on Computational Geometry (SoCG 2021).

Editors: Kevin Buchin and Éric Colin de Verdière; Article No. ; pp. :1-:37

Leibniz International Proceedings in Informatics



LIPICs Schloss Dagstuhl – Leibniz-Zentrum für Informatik, Dagstuhl Publishing, Germany



17 **1** Introduction

18 Given a surface represented in \mathbb{R}^3 as the zero set of a function $f : \mathbb{R}^3 \rightarrow \mathbb{R}$, the goal of
 19 isosurfacing is to find a piecewise linear (PL) approximation of the surface. This question
 20 naturally extends to isomanifolds of higher dimensions and codimensions defined as the zero
 21 set of multivariate multivalued smooth functions $f : \mathbb{R}^d \rightarrow \mathbb{R}^{d-n}$. Isosurfaces play a crucial
 22 role in medical imaging, computer graphics and geometry processing [36]. Higher dimensional
 23 isomanifolds are also of fundamental importance in many fields like statistics [16], dynamical
 24 systems [41], econometrics, or mechanics [36].

25 **State-of-the-art.** The most widely used algorithm to trace isomanifolds is the Marching
 26 Cube (MC) algorithm and its numerous variants [29, 44]. The MC algorithm uses a cubical
 27 grid to tessellate the ambient space. In many applications in 3-dimensions, the ambient space
 28 is decomposed into unstructured tetrahedral meshes, which led to the development of a
 29 variant of the MC algorithm named the Marching Tetrahedra algorithm. In higher dimensions,
 30 any tessellation of the ambient space has a complexity that depends exponentially on the
 31 ambient dimension. Hence a key to extending marching algorithms to higher dimensions is
 32 to circumvent the curse of dimensionality by using an *implicit* representation of the ambient
 33 tessellation. This is impossible for general triangulations but easy to do if one uses a grid.
 34 However, using a grid has other drawbacks and is not sufficient to break the exponential
 35 barrier. The reason for this is that the number of configurations inside a cubical cell grows
 36 exponentially with the dimension [44]. Hence the most promising approach seems to be to
 37 subdivide the ambient space \mathbb{R}^d using a highly regular triangulation such as the Freudenthal-
 38 Kuhn triangulation. Some early work along this direction has been published in Applied
 39 Mathematics [2, 25, 41], and a slightly more recent paper by Dobkin et al. [23] attracted the
 40 interest of the Computer Graphics community to the related Coxeter triangulations. Dobkin
 41 et al. however only considered the case of curves ($n = 1$). The most advanced work we are
 42 aware of is due to Min [35]. Min’s method uses the Freudenthal-Kuhn triangulation over a
 43 dyadic grid of \mathbb{R}^d and applies to isomanifolds of any dimension and codimension. The time
 44 complexity of Min’s method is, with our notations, $O(\delta^n \log \delta)$, where $\delta = 1/D$ and D is the
 45 maximal diameter of the simplices. The ambient dimension d is a constant hidden in the
 46 big O . The fact that the exponent of δ is the intrinsic dimension n , and not the ambient
 47 dimension d is a clear improvement over earlier methods. However, although not explicitly
 48 analysed by Min, the complexity in d remains exponential, and the method seems to be
 49 limited to small ambient dimensions. Experimental results are only reported in 3, and 4D.

50 **Contributions.** This paper discusses an efficient algorithm to compute a PL-approximation
 51 of isomanifolds. We extend the work of Dobkin et al. [23] and describe a simple algorithm
 52 to trace an n -dimensional isomanifold \mathcal{M} of \mathbb{R}^d for arbitrary n and d . Our algorithm uses
 53 any triangulation of a family of regular triangulations of \mathbb{R}^d that includes the Coxeter and
 54 the Freudenthal-Kuhn triangulations. Contrary to Min [35], our results are obtained with
 55 a uniform triangulation leading to a very simple algorithm. Key to our results, is a data
 56 structure that can implicitly store the full facial structure of such triangulations. The data
 57 structure is very compact and allows to retrieve the faces or the cofaces of a simplex of any
 58 dimension in an output sensitive way. Using this data structure, one can trace a connected
 59 submanifold of \mathbb{R}^d , starting from a given initial point on the manifold (Section 3). Our
 60 algorithm produces a PL-approximation of size polynomial in d and $\delta = 1/D$, and exponential
 61 in n . The complexity of the algorithm is also polynomial in d , and δ , and exponential in n .

62 Moreover, by taking δ large enough, the PL-approximation output by the algorithm is a
 63 faithful approximation of the isomanifold. Specifically, as shown in the full version of [13]
 64 and recalled in Section 2.2, if we take $\delta = \Omega(d^{2.5})$, the PL-approximation $\hat{\mathcal{M}}$ is $O(D^2)$ -
 65 close and isotopic to the isomanifold. Here the constants in the O depend on f and its
 66 derivatives. Hence, our algorithm constructs geometrically close and topologically correct
 67 PL-approximation of isomanifolds of bounded complexity in polynomial time.

68 Our algorithm can be extended in several directions. First, the dependency on d in the size
 69 of $\hat{\mathcal{M}}$ can be completely removed by combining our algorithm with dimensionality reduction
 70 (Section 3.4). We can also extend the algorithm to the case of isomanifolds with boundary
 71 and, more generally, to stratifolds (Section 3.5).

72 The algorithm has been implemented. In Section 4, we report on experimental results
 73 which show that the algorithm is practical and can handle cases that are far 16 ahead of the
 74 state-of-the-art. We also present an application in Algebraic Geometry that was used to verify
 75 a conjecture on projective varieties defined by polynomial equations in the complex projective
 76 plane. Following numerous experiments on various projective varieties, the conjecture was
 77 ultimately proved by Alvarez and Deroin [4].

78 The approximation of a manifold that is the zero set of a function is an example of the more
 79 general question of how to triangulate a manifold which has a long history in Mathematics.
 80 In particular, Whitney [45] introduced a construction that has some similarity with the
 81 present algorithm (see [10]). A major difference though is that topological guarantees can
 82 only be obtained if some intricate perturbations of the ambient triangulation are performed
 83 (Section 5). These techniques are at the moment incompatible with polynomial complexity.

84 **2 Background**

85 **2.1 Permutahedral representation of CFK-triangulations**

86 In this section, we give the most important definitions and basic properties of Coxeter and
 87 Freudenthal-Kuhn triangulations. An extensive discussion can be found in Appendix A.1.
 88 Both Coxeter and Freudenthal-Kuhn triangulations can be described as an arrangement of
 89 hyperplanes. They are related by an affine transformation. Let E be a finite set of vectors of
 90 \mathbb{R}^d and consider the set of hyperplanes $H_E = \{x \in \mathbb{R}^d \mid \langle x, u \rangle = k, u \in E, k \in \mathbb{Z}\}$. Let, in
 91 addition, H be the hyperplane of \mathbb{R}^{d+1} of equation $\langle x, \mathbf{1} \rangle = 0$ where $\mathbf{1}$ is the vector of \mathbb{R}^{d+1}
 92 whose coordinates are all 1.

93 **► Definition 1.** *The Freudenthal-Kuhn triangulation is the hyperplane arrangement $\mathcal{H}_{E_{FK}}$
 94 associated to the set of vectors $E_{FK} = \{e_1, \dots, e_d\} \cup \{u_{i,j} = e_j - e_i \mid 1 \leq i < j \leq d\}$. The
 95 Coxeter triangulation of type \tilde{A}_d is the hyperplane arrangement \mathcal{H}_{E_C} in \mathbb{R}^{d+1} associated to
 96 the set of vectors $E_C = \{r_{i,j} = e_i - e_{j+1} \mid 1 \leq i \leq j \leq d\}$, restricted to $H \simeq \mathbb{R}^d$.*

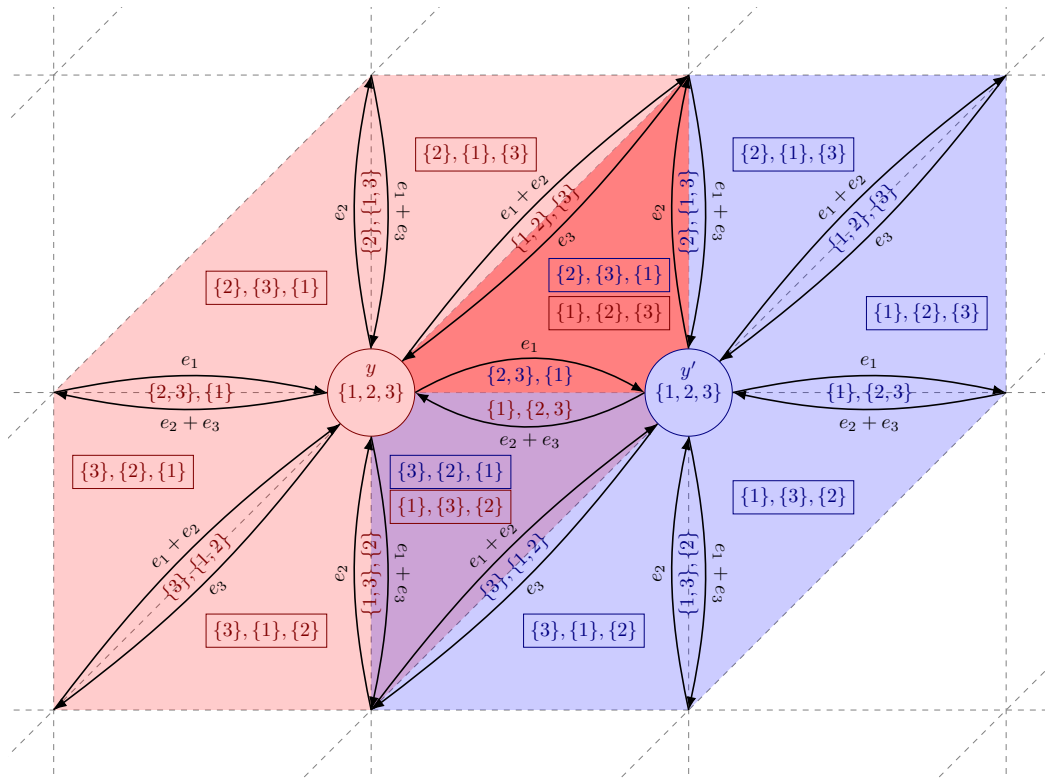
97 Two important facts follows. On one hand, because Coxeter and Freudenthal-Kuhn triangu-
 98 lations are related by an affine transformation, they have the same combinatorial structure.
 99 We call any triangulation that is the image of a Freudenthal-Kuhn triangulation under an
 100 affine transformation a CFK-triangulation. In this paper, we restrict our attention to Coxeter
 101 and Freudenthal triangulations since they are the simplest, but any CFK-triangulation could
 102 be used. The second fact is that each simplex in such a triangulation can be represented as
 103 a cell in an arrangement of $d(d-1)/2$ families of parallel hyperplanes which are known and
 104 do not need to be stored.

105 The next crucial observation relates CFK-triangulations and permutahedra, which allows
 106 to represent CFK-triangulations in a compact way (The definition and some combinatorial

107 properties of permutahedra are given in Appendix A.1.1). We first recall that two complexes
 108 are dual if there is a bijection between their faces that inverses the inclusion relationships.

109 ► **Proposition 2.** *The star of a vertex in a CFK-triangulation is combinatorially dual to a*
 110 *permutahedron.*

111 Since the facial structure of a permutahedron is fully described by ordered partitions, any
 112 simplex σ in a CFK-triangulation is characterized by a star that contains σ and by the
 113 ordered partition that specifies which simplex in the star is precisely σ . Since a simplex
 114 appears in several stars, we take the one that is centered at the lowest vertex of σ in the
 115 lexicographic order. This representation is called the permutahedral representation of a
 116 CFK-triangulation, see Figure 1. We further have:



117 ■ **Figure 1** The permutahedral representation of the simplices in the stars of vertices y and y' .

118 ► **Lemma 3 (Face computation).** *Let σ be an l -simplex in the FK-triangulation of \mathbb{R}^d .*
 119 *Computing all its k -faces can be done in time $O(ds)$, where $s = \binom{l+1}{k+1}$ is the number of*
 120 *k -faces of an l simplex. The space complexity of the algorithm is $O(l)$.*

121 ► **Lemma 4 (Coface computation).** *Let σ be a k -simplex in the FK-triangulation of \mathbb{R}^d given*
 122 *by its permutahedral representation. Computing the permutahedral representations of all its*
 123 *l -cofaces can be done in time $O(ds)$, where $s \leq \frac{1}{2^{\min(l,d-l)}} \binom{d-k}{d-l} (d-k+1)!$ is the number of*
 124 *l -cofaces of a k -simplex in the FK-triangulation. The space complexity of the algorithm is*
 125 *$O(d)$.*

126 **2.2 PL-approximation of isomanifolds**

127 We first recall sufficient conditions under which the PL-approximation $\hat{\mathcal{M}}$ output by the
 128 algorithm faithfully reproduces the original isomanifold. These conditions are fully described
 129 in the full version of [13] and we simply state here the main results specialized to the case of
 130 CFK-triangulations.

131 We will say that f has *bounded complexity* if the three following quantities γ_{\max} , λ_{\min} and
 132 α_{\max} are positive and bounded.

133
$$\gamma_{\max} = \max_{x \in \mathcal{T}_0} (\max_i |\text{grad} f^i(x)|) \quad \lambda_{\min} = \min_{x \in \mathcal{T}_0} \lambda_{\min}(x), \quad \alpha_{\max} = \max_{x \in \mathcal{T}_0} \max_i \|\text{Hes}(f^i)(x)\|_2$$

134 where

- 135 ■ \mathcal{T}_0 denotes the set of all $\sigma \in \mathcal{T}$, such that $(f^i)^{-1}(0) \cap \sigma \neq \emptyset$ for all i .
- 136 ■ $\text{grad} f^i = (\partial_j f^i)_j$ denotes the gradient of component f^i , for $i \in [1, d - n]$,
- 137 ■ $\text{Gram}(\nabla f)$ denotes the Gram matrix whose elements are $\nabla f^i \cdot \nabla f^j$ where \cdot stands for
 138 the dot product.
- 140 ■ $\lambda_{\min}(x)$ denotes the smallest absolute value of the eigenvalues of $\text{Gram}(\nabla f(x))$,¹
- 141 ■ $\text{Hes}(f) = (\partial_k \partial_l f^i)_{k,l}$ denotes the Hessian matrix of second order derivatives,
- 143 ■ $|\cdot|$ denotes the Euclidean norm of a vector and $\|\cdot\|_2$ the operator 2-norm of a matrix.²

144 We can now restate the topological result of [13] :

145 ► **Theorem 5.** *Assume that the function f has bounded complexity. If the precision of the*
 146 *CFK-triangulation satisfies $D = O(d^{-5/2})$, where the constant in the big O depends on γ_{\max} ,*
 147 *λ_{\min} and α_{\max} , then $\hat{\mathcal{M}}$ is a manifold isotopic to the zero set \mathcal{M} of f .*

148 Moreover, we can bound the Fréchet distance between \mathcal{M} and $\hat{\mathcal{M}}$. The Fréchet distance is a
 149 quite strong notion of distance and, in particular, it bounds the Hausdorff distance.

150 ► **Definition 6** (Fréchet distance for embedded manifolds). *Let \mathcal{M}_a and \mathcal{M}_b be two homeo-*
 151 *morphic, compact submanifolds of \mathbb{R}^d . Write \mathcal{H} for the set of all homeomorphisms from \mathcal{M}_a to*
 152 *\mathcal{M}_b . The Fréchet distance between \mathcal{M}_a and \mathcal{M}_b is $d_F(\mathcal{M}_a, \mathcal{M}_b) = \inf_{h \in \mathcal{H}} \sup_{x \in \mathcal{M}_a} d(x, h(x))$.*

153 ► **Theorem 7.** *Assume that the function f has bounded complexity. Then, $d_F(\mathcal{M}, \hat{\mathcal{M}}) =$
 154 $O(D^2)$ where the constant in the big O depends on γ_{\max} , λ_{\min} and α_{\max} .*

155 **3 Tracing isomanifolds**

156 In this section, we describe an algorithm that computes a PL-approximation $\hat{\mathcal{M}}$ of an
 157 isomanifold \mathcal{M} . The algorithm has some similarity with the Marching Cube algorithm [33]
 158 but departs from it in two fundamental ways. First, because of the curse of dimensionality,
 159 we cannot afford to look at all the cells in the grid and need to limit the search to cells
 160 that are close to \mathcal{M} . The problem of computing $\hat{\mathcal{M}}$ can be naturally decomposed into two
 161 subproblems: locating the various components of \mathcal{M} (i.e., finding at least one point in each
 162 connected component), and then tracing around each component, using the fact that the
 163 components are connected. This decomposition is used by various authors, see for example
 164 [44, 23]. In this paper, we focus on the tracing problem, although we discuss very briefly

139 ¹ Because a Gram matrix is a symmetric square matrix, its eigenvalues are well defined and real.

142 ² The operator norm is defined as $\|A\|_p = \max_{x \in \mathbb{R}^n} \frac{|Ax|_p}{|x|_p}$, with $|\cdot|_p$ the p -norm on \mathbb{R}^n .

165 (Section 3.2) the problem of locating the components. As pointed out by Dobkin et al. many
 166 applications supply their own starting points.

167 The second major difference with the original marching cube algorithm is to replace the
 168 usual cubical grid by a CFK-triangulation of the ambient space. Taking a CFK-triangulation
 169 instead of a grid is a major advantage in high dimensions that has been recognized in the
 170 pioneering works of Allgower, and Schmidt [3] and of Dobkin et al. [23], see also [35]. The
 171 novelty here is to use the data structure of Section 2.1 to represent a CFK-triangulation. As
 172 a consequence, we will keep two main advantages of using grids: very limited storage and
 173 fast basic operations.

174 3.1 Isomanifolds

175 Let $f : \mathbb{R}^d \rightarrow \mathbb{R}^{d-n}$ be a smooth (C^2 suffices) function, and suppose that 0 is a regular value
 176 of f , meaning that at every point x such that $f(x) = 0$, the Jacobian of f is non-degenerate.
 177 Then the zero set of f is an n -dimensional manifold as a direct consequence of the implicit
 178 function theorem, see for example [24, Section 3.5]. We further assume that $f^{-1}(0)$ is compact.
 179 As in [1] we consider a triangulation \mathcal{T} of \mathbb{R}^d . The function \hat{f} is the linear interpolation of
 180 the values of f at the vertices if restricted to a single simplex $\sigma \in \mathcal{T}$, i.e.

$$181 \quad \forall x \in \sigma : \hat{f}(x) = \sum_{v \in \sigma} \lambda_v(x) f(v), \quad (1)$$

182 where the λ_v are the barycentric coordinates of x with respect to the vertices v of σ . For
 183 any function $g : \mathbb{R}^d \rightarrow \mathbb{R}^{d-n}$ we write g^i , with $i = 1, \dots, d-n$, for the components of g .

184 The PL-approximation is now defined as $\hat{f}^{-1}(0) = \hat{\mathcal{M}}$. Locally, $\hat{f}|_{\sigma}^{-1}(0)$ is generically the
 185 intersection of an n -flat H_{σ} with σ . More precisely we note that $\hat{f}|_{\sigma}^{-1}(0)$ is an n -flat if the
 186 gradients of $\hat{f}^i|_{\sigma}$ are linearly independent, which can be easily achieved by perturbing f
 187 infinitesimally (or at least its values at the vertices). Let τ_j^{d-n} and τ_j^{d-n-1} be faces of σ of
 188 dimension $d-n$ and $d-n-1$. An infinitesimal perturbation of f , can prevent either $\hat{f}|_{\sigma}^{-1}(0)$
 189 from intersecting the faces τ_j^{d-n-1} , or the gradients of $\hat{f}^i|_{\sigma}$ and the normal spaces of τ_j^{d-n}
 190 (for each fixed j) from failing to span \mathbb{R}^d . More precise statements on the geometric and
 191 topological stability of the triangulation under perturbations of f can be found in the full
 192 version of [13, Section 5]. Because $\hat{f}|_{\sigma}^{-1}(0)$ is (generically) the intersection of an n -flat (H_{σ})
 193 and σ , it is an n -dimensional polytope denoted by C_{σ} . The PL-approximation or mesh $\hat{\mathcal{M}}$
 194 of \mathcal{M} is the polytopal cell complex obtained by gluing the polytopes C_{σ} associated to all the
 195 simplices σ in \mathcal{T} .

196 3.2 Manifold tracing algorithm

197 Let \mathcal{M} be the zero set of some function $f : \mathbb{R}^d \rightarrow \mathbb{R}^{d-n}$, and let $\hat{\mathcal{M}}$ be the associated
 198 PL-approximation defined over a triangulation \mathcal{T} of the ambient space \mathbb{R}^d . Both n , and d are
 199 known but arbitrary, and will be considered as parameters in the complexity analysis. We
 200 write $k = d-n$ for the codimension of \mathcal{M} . The algorithm will use for \mathcal{T} a CFK-triangulation
 201 stored using the data structure from Section A.1. We assume that the manifold $\hat{\mathcal{M}}$, and the
 202 triangulation \mathcal{T} satisfy the following genericity hypothesis:

203 **► Hypothesis 8 (Genericity).** *Let σ be a d -simplex of \mathcal{T} that intersects H_{σ} . No subface of σ*
 204 *of dimension less than k intersects H_{σ} , and any subface of σ of dimension k intersects H_{σ}*
 205 *in at most one point and transversally.*

206 We note that this condition can be satisfied by an infinitesimal perturbation for isomanifolds.
 207 This requires some explanation. We recall that the CFK-triangulation is a hyperplane
 208 arrangement, and up to translation there are a finite number of k -flats that contain all
 209 k -simplices in the CFK triangulation. Hypothesis 8 is not satisfied, if either the flat H_σ
 210 is not linearly independent of these k -flats, or if H_σ does intersect some $(k - 1)$ -flat in
 211 the CFK-triangulation. In the previous section, we have already seen that an infinitesimal
 212 perturbation ensures that H_σ is n -dimensional. Because two affine spaces whose dimensions
 213 do not add up to the ambient dimension don't intersect with generically and two affine
 214 spaces whose dimensions add up to exactly the ambient dimension intersect in a single point,
 215 we see that genericity can be achieved by perturbing f infinitesimally. We further remark
 216 that, generically, any vertex of the PL-approximation $\hat{\mathcal{M}}$ is the intersection point between a
 217 k -simplex σ of \mathcal{T} with the n -flat H_σ that interpolates f inside σ .

218 **Algorithm 1** Manifold tracing algorithm

218 **input** : the permutahedral representation of a triangulation \mathcal{T} of \mathbb{R}^d ,
 219 the codimension of the isomanifold $k = d - n$,
 220 a seed k -simplex τ_0 that intersects $\hat{\mathcal{M}}$
 221 **oracle** : Given a k -simplex σ of \mathcal{T} , decide whether σ intersects H_σ and, in the
 affirmative, report the corresponding vertex $\sigma \cap H_\sigma = \sigma \cap \hat{\mathcal{M}}$.
 222 **output** : Set \mathcal{S} of the simplices in \mathcal{T} of dimension k that intersect $\hat{\mathcal{M}}$, represented by
 their permutahedral representation, and the corresponding set $\hat{\mathcal{M}}_0$ of
 intersection points

223 Initialize the queue \mathcal{Q} and the set \mathcal{S} with τ_0
 224 **while** the queue \mathcal{Q} is not empty **do**
 225 Pop a k -dimensional simplex τ from \mathcal{Q}
 226 **foreach** cofacet ϕ of τ **do**
 227 **foreach** facet σ of ϕ **do**
 228 **if** σ does not lie in \mathcal{S} and intersects $\hat{\mathcal{M}}$ (which can be decided using the
 oracle) **then**
 229 Insert σ into the queue \mathcal{Q}
 230 Insert σ into \mathcal{S} together with the intersection point provided by the
 oracle

219 The algorithm essentially computes the set \mathcal{S} of k -simplices of \mathcal{T} that intersect $\hat{\mathcal{M}}$. The
 220 elements of \mathcal{S} are in 1-1 correspondence with the vertices of $\hat{\mathcal{M}}$ thanks to the Genericity
 221 hypothesis. The so-called intersection oracle is a basic ingredient of the algorithm:

222 **Intersection oracle:** Given a k -simplex σ of \mathcal{T} , decide whether σ intersects H_σ and, in the
 223 affirmative, report the corresponding vertex $\sigma \cap H_\sigma$.

224 It is easy to see that the intersection oracle reduces to solving a linear system. Indeed,
 225 generically, a vertex is the intersection of a k -simplex σ of \mathcal{T} with the m -flat H_σ that
 226 interpolates f inside σ . One can compute the barycentric coordinates of $\sigma \cap H_\sigma$ by solving
 227 a linear system of k equations, and k unknowns. It then remains to check whether the
 228 barycentric coordinates are all non-negative (to ensure that the intersection point lies inside
 229 σ). It follows that the intersection oracle reduces to evaluating f at the $k + 1$ vertices of σ
 230 plus solving a $k \times k$ linear system.

231 In addition, we need to provide a set of k -simplices of \mathcal{T} to initialize the tracing. These
 232 simplices must intersect all the connected components of the isomanifold and are called

233 seed simplices. If \mathcal{M} consists of multiple connected components, then a seed simplex must
 234 be provided per each connected component and we proceed in the same manner for each
 235 component. So we will assume for now that \mathcal{M} is connected.

236 The seed simplices are given as part of the input and we don't discuss in this paper the
 237 problem of their construction. We simply observe that they can be obtained by computing a
 238 critical point (e.g., a point with smallest x_1 -coordinate) on each connected component of the
 239 isomanifold, which reduces to finding a solution to a system of equations, on which a large
 240 body of literature exists. See for example [38, 37, 23] and also the discussion in Wenger's
 241 book [44, Section 8.4]. Once such a seed point has been computed, we simply translate
 242 and rotate the triangulation \mathcal{T} so that the seed point coincides with the barycenter of a
 243 k -simplex of \mathcal{T} and the intersection with the manifold is transversal as demanded by the
 244 genericity hypothesis (for numerical stability it is convenient if the angle between the tangent
 245 space of the manifold and the starting k -simplex is large, which is easy to ensure). If the
 246 distance between \mathcal{M} and $\hat{\mathcal{M}}$ is small enough, then $\hat{\mathcal{M}}$ also intersects the same k simplex, see
 247 Section 2.2.

248 The algorithm is described as Algorithm 1. It takes as input the permutahedral representation
 249 of an ambient FKC-triangulation \mathcal{T} and a seed k -simplex τ_0 of \mathcal{T} . We assume that \mathcal{T} satisfies
 250 the Genericity Hypothesis 8, which can be enforced by infinitesimal perturbations of f as
 251 discussed in Section 3.1.

252 The algorithm maintains the subset \mathcal{S} of the simplices in \mathcal{T} of dimension k that intersect $\hat{\mathcal{M}}$.
 253 \mathcal{S} is initialized with the seed simplex τ_0 and stored as a hash table so that we can decide in
 254 constant time if a given k -simplex belongs to \mathcal{S} . Then, starting from τ_0 , we look at all its
 255 cofacets and consider all the facets of those cofacets that are not in \mathcal{S} (i.e. they have not
 256 been considered yet). This can be done using a queue \mathcal{Q} of candidate k -simplices. Each of
 257 these simplices is queried with the intersection oracle and, if it is found to intersect $\hat{\mathcal{M}}$, it
 258 is added to \mathcal{S} if not already present. Upon termination, \mathcal{S} contains all the k -dimensional
 259 simplices of \mathcal{T} that intersect $\hat{\mathcal{M}}$. Each such intersection, which consists of a single point (by
 260 the Genericity hypothesis), is a vertex of $\hat{\mathcal{M}}$. Hence $\hat{\mathcal{M}}_0$ is the vertex set of $\hat{\mathcal{M}}$.

261 Note that our algorithm essentially traverses the adjacency graph of the k and $(k+1)$ -simplices
 262 of \mathcal{T} that intersect $\hat{\mathcal{M}}$. It therefore identifies not only the set $\hat{\mathcal{M}}_0$ of vertices of $\hat{\mathcal{M}}$, but also
 263 the edges joining two such vertices (associated to the cofacets of the k -simplices in \mathcal{S}). By
 264 simply reporting those cofacets on the fly, the algorithm can output the 1-skeleton $\hat{\mathcal{M}}_1$ of
 265 the n -dimensional polytopal cell complex $\hat{\mathcal{M}}$. The higher dimensional faces of $\hat{\mathcal{M}}$ are the
 266 polytopes $C_\tau = \tau \cap H_\tau$ for all the cofaces τ of the k -simplices of \mathcal{S} . If needed, the full Hasse
 267 diagram of $\hat{\mathcal{M}}$ can be computed from $\hat{\mathcal{M}}_0$. This can be done in an output sensitive manner
 268 by using the permutahedral representation of \mathcal{T} and the algorithm of Section A.1 to compute
 269 cofaces by increasing dimensions.

270 3.3 Complexity analysis

271 We can easily bound the complexity of the manifold tracing algorithm as a function of the
 272 size of the output.

273 **► Proposition 9.** *The time complexity of the algorithm is $O(k2^n I|\mathcal{S}|)$ where I is the time
 274 complexity of one call of the intersection oracle, and $|\mathcal{S}|$ is the number of simplices of
 275 dimension k output by the algorithm.*

276 Since, the intersection oracle reduces to evaluating f at the $k+1$ vertices of σ plus solving a
 277 $k \times k$ linear system, $I = O(k^\omega)$ where $\omega \approx 2.375$.

278 We will now express the size of the output in terms of quantities that depend on the manifold,
 279 the ambient dimension d , and the resolution of the triangulation (the diameter D of a simplex)
 280 which bounds the density of the output sample, and the precision of the approximation. Our
 281 result holds for K -sparse manifolds, i.e. submanifolds whose intersection with any k -flat
 282 consists of at most K points. In practical situations, K is usually small and, in particular,
 283 K is a constant for algebraic isomanifolds of bounded degree.

284 ► **Proposition 10** (Size of the output). *Assume that \mathcal{M} is contained in the unit cube $C_d =$
 285 $[0, 1]^d$, and that any k -flat intersects \mathcal{M} at most K times. Writing $|\mathcal{S}| = N_C$ when \mathcal{T} is
 286 a Coxeter triangulation and $|\mathcal{S}| = N_{FK}$ for a Freudenthal triangulation, we have $N_C \leq$
 287 $\frac{K}{n!} \times \left(\frac{d^2 \sqrt{d(d+2)}}{2\sqrt{2}D}\right)^n$ and $N_{FK} \leq \frac{K}{n!} \times \left(\frac{d^3}{\sqrt{2}D}\right)^n$ where D is the diameter of a simplex of \mathcal{T} .*

288 We see that Coxeter triangulations lead to smaller samples than FK-triangulations by a
 289 factor of roughly 2^n . This will be confirmed experimentally (see Figure 3).

290 As noticed in Section 3.2, a simple variant of the algorithm can compute the full Hasse diagram
 291 of $\hat{\mathcal{M}}$ in an output sensitive manner. The following lemma shows that the combinatorial
 292 complexity of $\hat{\mathcal{M}}$ is of the same order as the combinatorial complexity as $\hat{\mathcal{M}}_0$.

293 ► **Proposition 11.** *The combinatorial complexity of $\hat{\mathcal{M}}$ is $|\mathcal{S}| \times \left(\frac{3}{2}\right)^n (n+1)!$, where $|\mathcal{S}|$ is
 294 bounded in Proposition 10. If $n = O(1)$, the combinatorial complexity of $\hat{\mathcal{M}}$ is polynomial in
 295 d , and $\delta = 1/D$.*

296 We combine Propositions 9, 10, and 11 to obtain our main result.

297 ► **Theorem 12.** *Assume that \mathcal{M} is contained in the unit cube $[0, 1]^d$ and that any affine
 298 k -flat intersects \mathcal{M} at most K times (K is usually small, and is in particular a constant for
 299 algebraic isomanifolds of bounded degree). Let, in addition, D be the precision required on the
 300 approximation (the diameter of a simplex in the ambient triangulation \mathcal{T}). The size of the
 301 output, and the time complexity of the algorithm are polynomial in the ambient dimension d ,
 302 and in $\delta = 1/D$, and exponential in the intrinsic dimension n . The same result holds for the
 303 full PL-approximation $\hat{\mathcal{M}}$ of \mathcal{M} .*

304 3.4 Dimensionality reduction

305 As seen from Proposition 10, the size $|\mathcal{S}|$ of the output of the algorithm, considered as a
 306 function of the resolution D of the triangulation, depends exponentially on n (which is to be
 307 expected), and only polynomially on d (which is fortunate). Nevertheless, the computing
 308 time of our algorithm and the size of the output depend on d . Removing the dependency on
 309 d in the time complexity is impossible since we need to evaluate a vector-valued function f
 310 at a number of points of \mathbb{R}^d , which takes $\Omega(d)$ time per evaluation. However, we will see
 311 that we can reduce the size of the mesh produced by our algorithm.

312 Examples of samples of \mathcal{M} whose sizes depend on n but not on d , and lead to good
 313 approximations are known. Especially important are D -nets [17, 9]. A D -net consists of
 314 a finite number of sample points of \mathcal{M} such that no point of \mathcal{M} is at distance more than
 315 D from a sample point (density condition), and no two sample points are closer than cD
 316 for some positive constant c (separation condition). A simple volume argument shows that
 317 the size of a D -net of a n -dimensional smooth submanifolds is $O(1/D^n)$ [8, Lemma 5.3].
 318 The sample produced by our algorithm is D -dense on the piecewise linear approximation.
 319 This implies that we have a sample that has a Hausdorff distance of $D + d_F(\mathcal{M}, \hat{\mathcal{M}})$ to the
 320 manifold, where $d_F(\mathcal{M}, \hat{\mathcal{M}})$ is bounded in Theorem 7.

321 Since its cardinality depends on d , it is not well separated and, in particular, not a D -net of
 322 \mathcal{M} . If we are mostly interested in the output sample, we can easily sparsify it to obtain a
 323 D -net. However, by doing so, we will lose the combinatorial structure of the mesh.

324 We now show how to compute a D -dense sample of \mathcal{M} of size independent of d , together
 325 with a mesh. Specifically, we will reduce dimensionality using a variant of the celebrated
 326 Johnson-Lindenstrauss lemma for manifolds. Doing so, we depart from our previous worst-
 327 case analysis by allowing some approximation factor ε and tolerate a guarantee that holds
 328 only with high probability.

329 ► **Theorem 13** (Johnson-Lindenstrauss lemma for manifolds [20, 42]). *Pick any $\varepsilon, \eta > 0$,
 330 and let $d' = \Omega\left(\frac{n}{\varepsilon^2} \log \frac{1}{\varepsilon} + \frac{1}{\varepsilon^2} \log \frac{\Gamma}{\eta}\right)$, where Γ is a quantity that depends only on intrinsic
 331 properties of \mathcal{M} . Let Φ be the projection on a random affine subspace of dimension d' . Then,
 332 with probability $> 1 - \eta$, for all $x, y \in \mathcal{M}$, we have $(1 - \varepsilon) \sqrt{\frac{d'}{d}} \leq \frac{\|\Phi x - \Phi y\|}{\|x - y\|} \leq (1 + \varepsilon) \sqrt{\frac{d'}{d}}$.*

333 Let $\Psi = \sqrt{\frac{d'}{d}} \Phi$. By the theorem, the image $\Psi(\mathcal{M})$ of \mathcal{M} is a submanifold of dimension n
 334 embedded in $\mathbb{R}^{d'}$. One can now run the manifold tracing algorithm in $\mathbb{R}^{d'}$ to sample, and
 335 mesh $\Psi(\mathcal{M})$. The algorithm works as described before except that we need another oracle
 336 that, given a $(d' - n)$ -simplex σ of the CFK-triangulation of $\mathbb{R}^{d'}$, decides whether its inverse
 337 image $\Psi^{-1}(\sigma)$ intersects \mathcal{M} or not. Note that $\Psi^{-1}(\sigma)$ is a $(d - d')$ -dimensional flat strip
 338 (that is the product of a face and an affine subspace) in \mathbb{R}^d , and that the complexity of this
 339 new oracle is the same as the complexity of the basic intersection oracle, i.e. polynomial in d .
 340 Due to the scaling factor $\sqrt{d/d'}$, the resolution of the triangulation in the low dimensional
 341 space $\mathbb{R}^{d'}$ has to be scaled by the same factor if one wants to satisfy a given sampling density
 342 on \mathcal{M} . Since the geometry of the manifold is also scaled in the same way [26], the analysis
 343 of the algorithm will be unchanged. Proposition 10 then shows that the size of the output
 344 sample does not depend on d but only on n and D for fixed ε , and η . Moreover, since the
 345 complexities of the projection and of the new oracle are polynomial in d , Proposition 9
 346 implies that the overall complexity is still polynomial in d .

347 3.5 Isomanifolds with boundary, and isostratifolds

348 The case of isomanifolds with boundary and, more generally, of isostratifolds can be handled
 349 in very much the same way. By an isomanifold of dimension n with boundary, we mean that,
 350 on top of a function $f : \mathbb{R}^d \rightarrow \mathbb{R}^{d-n}$, we are given another function $f_\partial : \mathbb{R}^d \rightarrow \mathbb{R}$, and the set
 351 we consider is $\mathcal{M} = f^{-1}(0) \cap f_\partial^{-1}([0, \infty))$. We note that $\partial\mathcal{M} = f^{-1}(0) \cap f_\partial^{-1}(0)$.

352 Similarly to (1), we also define $\hat{f}_\partial|_\tau(x) = \sum_{v \in \sigma} \lambda_v(x) f_\partial(v)$. We write \hat{f} for the (global)
 353 piecewise linear function that coincides with $\hat{f}|_\tau$ on each τ of \mathcal{T} , and \hat{f}_∂ for the (global)
 354 piecewise linear function that coincides with $\hat{f}_\partial|_\tau$ on each τ of \mathcal{T} . We note that the piecewise
 355 linear approximation of the boundary $\partial\hat{\mathcal{M}} = \hat{f}_\partial^{-1}(0) \cap \hat{f}^{-1}(0)$ is a subset of $\hat{f}^{-1}(0)$, i.e. the
 356 piecewise linear approximation of the manifold ignoring the boundary. The piecewise linear
 357 approximation $\hat{\mathcal{M}}$ of the manifold with boundary consists of the following cells:

- 358 ■ For each τ of \mathcal{T} , such that $\hat{f}_\partial|_\tau$ is positive on τ , and $(\hat{f}|_\tau)^{-1}(0) \cap \tau \neq \emptyset$, we add
 359 $(\hat{f}|_\tau)^{-1}(0) \cap \tau$.
- 360 ■ For each τ of \mathcal{T} , such that $(\hat{f}|_\tau)^{-1}(0) \cap \tau \neq \emptyset$, and $(\hat{f}_\partial|_\tau)^{-1}(0) \cap \tau \neq \emptyset$, we add
 361 $(\hat{f}|_\tau)^{-1}(0) \cap (\hat{f}_\partial|_\tau)^{-1}([0, \infty)) \cap \tau$.

362 We will assume that the Genericity Hypothesis 8 holds for both $\hat{\mathcal{M}}$, and $\partial\hat{\mathcal{M}}$.

363 We can now adapt the algorithm of Section 3.2 as follows. In addition to reporting the set
 364 S_k of k -faces of the triangulation \mathcal{T} that intersect $\hat{\mathcal{M}}$, the algorithm will also report the set

365 S_{k+1} of $(k + 1)$ -faces of the triangulation \mathcal{T} that intersect $\partial\hat{\mathcal{M}}$. The computation of S_{k+1} is
 366 done by the following simple modification of Algorithm 1: if the k -dimensional facet σ of τ
 367 intersects $\hat{f}^{-1}(0)$ at a point x such that $\hat{f}_{\partial|\tau}(x) < 0$ (i.e. x is not in $\hat{\mathcal{M}}$), we then compute
 368 the intersection point of τ with $\hat{f}_{\partial}^{-1}(0)$, and put τ in S_{k+1} .

369 As for the case of manifolds without boundary (see the discussion at the end of Section 3.2),
 370 the algorithm traverses (and therefore computes) the 1-skeleton of $\hat{\mathcal{M}}$. Under the Genericity
 371 Hypothesis 8, the vertices of $\hat{\mathcal{M}}_1$ are in bijection with the simplices of $S_k \cup S_{k+1}$. The edges
 372 are obtained by applying the following rules below (we identify a simplex in S_k (resp. S_{k+1})
 373 and the intersection point $S_k \cap \hat{\mathcal{M}}$ (resp. $S_{k+1} \cap \partial\hat{\mathcal{M}}$):

- 374 1. Two simplices σ_1 , and σ_2 of S_k are joined by an edge in $\hat{\mathcal{M}}_1$ if and only if there exists a
 375 simplex in \mathcal{T}_{k+1} with faces σ_1 and σ_2 .
- 376 2. Two simplices τ_1 , and τ_2 of S_{k+1} are joined by an edge in $\partial\hat{\mathcal{M}}_1$ if and only if there exists
 377 a simplex in \mathcal{T}_{k+2} with faces τ_1 and τ_2 .
- 378 3. A simplex σ of S_k , and a simplex τ of S_{k+1} are joined by an edge in $\partial\hat{\mathcal{M}}_1$ if and only if
 379 σ is a facet of τ .

380 The three rules above together with the permutahedral representation of \mathcal{T} provide a way to
 381 construct the 1-skeleton of $\hat{\mathcal{M}}$ on the fly. The total cost is output sensitive. If needed, the
 382 entire combinatorial structure of $\hat{\mathcal{M}}$ can be computed by traversing the full triangulation \mathcal{T} .
 383 The above construction generalizes easily to arbitrary isostratifolds. Isostratifolds are
 384 stratified spaces that are defined by equations and inequalities. An example of such a
 385 stratifold is an octant of the sphere in \mathbb{R}^3 that can be defined by as $x^2 + y^2 + z^2 - 1 = 0$,
 386 $x \geq 0$, $y \geq 0$, and $z \geq 0$. We compute the 1-skeleton of $\hat{\mathcal{M}}$ and construct a graph whose
 387 nodes are the simplices of dimensions $k, k + 1, \dots, d$ that intersect the strata of dimension
 388 $n, n - 1, \dots, 0$.

389 4 Experimental results

390 The data structure of Section A.1 and the algorithm of Section 3 have been implemented in
 391 C++. The code is robust and fast and will be released in the GUDHI library [30]. Full detail
 392 on the implementation, including the implementation of the oracle, can be found in [32].

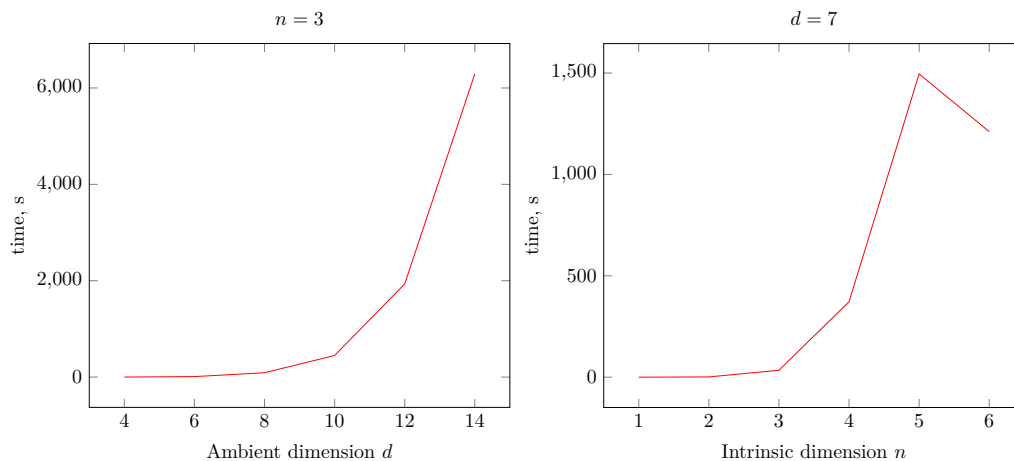
393 In this section, we explore the dependency of our C++ implementation of the data structure
 394 for the ambient CFK-triangulation, and of the manifold tracing algorithm on the properties
 395 of the triangulation, and of the input manifold.

396 4.1 Performance of the algorithm

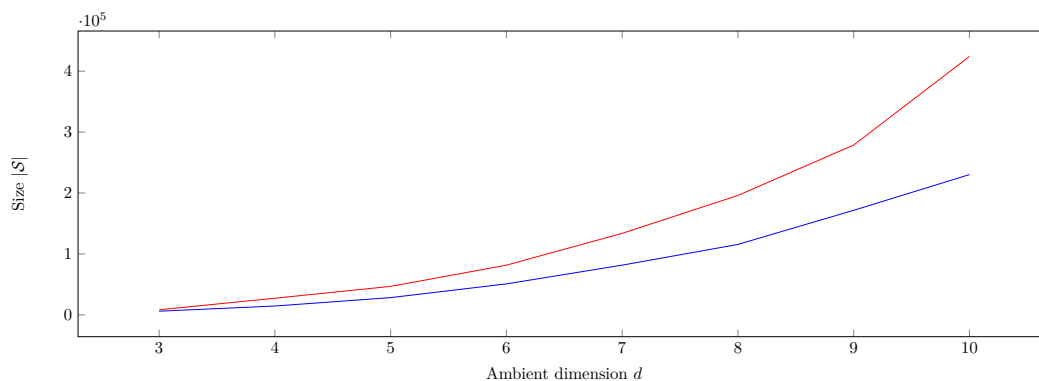
397 We show the performance of our implementation of the manifold tracing algorithm for
 398 various ambient and intrinsic dimensions in Figure 2. In Figure 3, we can see that using
 399 Coxeter triangulation is beneficial in practice as it produces a smaller output in less time
 400 (see Proposition 10).

416 In Figure 4, we present a PL approximation of a two-dimensional Clifford torus without
 417 boundary embedded in \mathbb{R}^{10} built by the manifold tracing algorithm. The torus has been
 418 rotated and translated in \mathbb{R}^{10} so that the coordinate axes do not play any special role. Note
 419 that there is no C^2 isometric embedding of the Clifford torus in \mathbb{R}^3 .

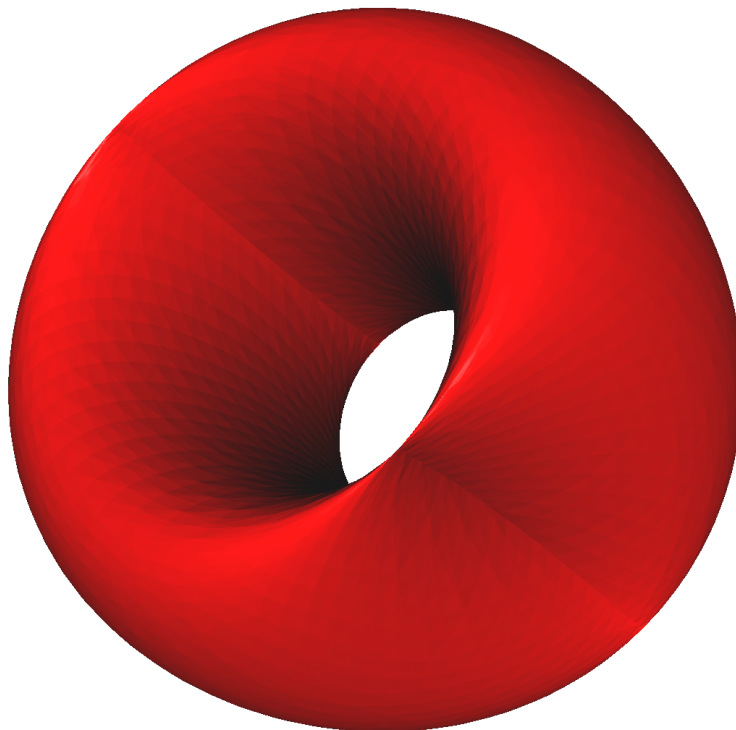
XX:12 Isomanifold Tracing in \mathbb{R}^d , using Coxeter-Freudenthal-Kuhn Triangulations



401 **Figure 2** The effect of the ambient dimension d and of the intrinsic dimension n on the computation
 402 time of the manifold tracing algorithm. The reconstructed manifold in the tests is the n -dimensional
 403 sphere embedded in \mathbb{R}^d . The ambient triangulation used is a Coxeter triangulation of type \tilde{A}_d . The
 404 diameter of the full simplices is fixed for all d .



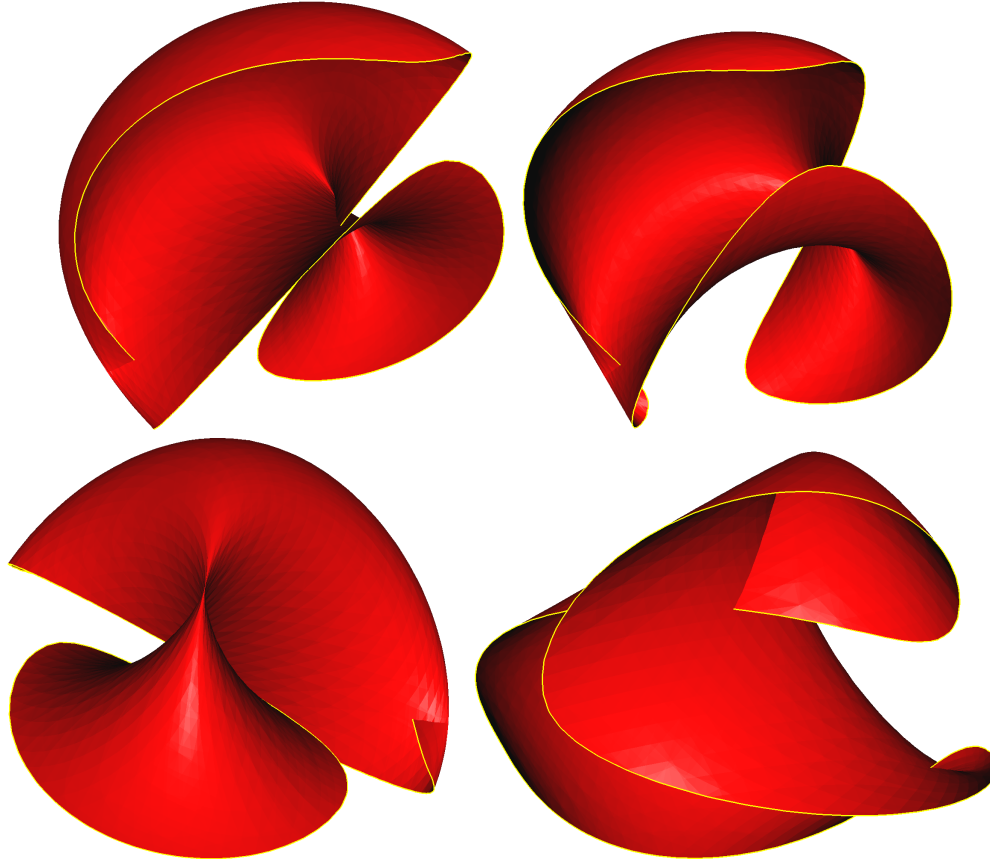
405 **Figure 3** Comparison of the size of the output of the manifold tracing algorithm using two
 406 types of ambient triangulations: a Coxeter triangulation of type \tilde{A}_d (in blue), and the Freudenthal-
 407 Kuhn triangulation of \mathbb{R}^d (in red) with the same diameter $0.07\sqrt{d}$ of d -dimensional simplices. The
 408 reconstructed manifold is the 2-dimensional implicit surface “Chair” embedded in \mathbb{R}^d given by the
 409 equations: $(x_1^2 + x_2^2 + x_3^2 - 0.8)^2 - 0.4((x_3 - 1)^2 - 2x_1^2)((x_3 + 1)^2 - 2x_2^2) = 0$, and $x_i = 0$ for $i > 3$.



410 ■ **Figure 4** The piecewise-linear approximation of a flat torus embedded in \mathbb{R}^{10} defined by the
411 equations $x_1^2 + x_2^2 = 1$, and $x_3^2 + x_4^2 = 1$, and $x_i = 0$ for $i > 4$, projected to \mathbb{R}^3 . The ambient
412 triangulation used is a Coxeter triangulation of type \tilde{A}_{10} with the diameter of the full-dimensional
413 simplices 0.23. The output size $|\mathcal{S}|$ is 509952. The execution time of the algorithm is 231s. The
414 torus has been rotated and translated in \mathbb{R}^{10} so that the coordinate axes do not play any special
415 role.

420 **4.2 Manifolds with boundary**

421 The algorithm has been adapted to handle submanifolds with boundary and surfaces with a
 422 piecewise smooth boundary, see Section 3.5. In Figure 5, we present the mesh obtained by
 423 our algorithm on a portion of a flat torus embedded in \mathbb{R}^4 , and cut by a hypersphere. The
 424 torus has been rotated and translated in \mathbb{R}^4 so that the coordinate axes do not play any
 425 special role.



426 ■ **Figure 5** Four views of the flat torus in \mathbb{R}^4 given by two equations $x_1^2 + x_2^2 = 1$, and $x_3^2 + x_4^2 = 1$ cut
 427 by the hypersphere $(x_1 - 1)^2 + x_2^2 + (x_3 - 1)^2 + x_4^2 = 4$, projected to \mathbb{R}^3 . The ambient triangulation used
 428 is a Coxeter triangulation of type A_4 with the diameter 0.15 of the full-dimensional simplices. The
 429 reconstructed boundary is highlighted in yellow. The size $|\mathcal{S}|$ of the piecewise-linear approximation
 430 is 14 779. The execution time of the algorithm is 1.84s. The torus has been rotated and translated
 431 in \mathbb{R}^4 so that the coordinate axes do not play any special role.

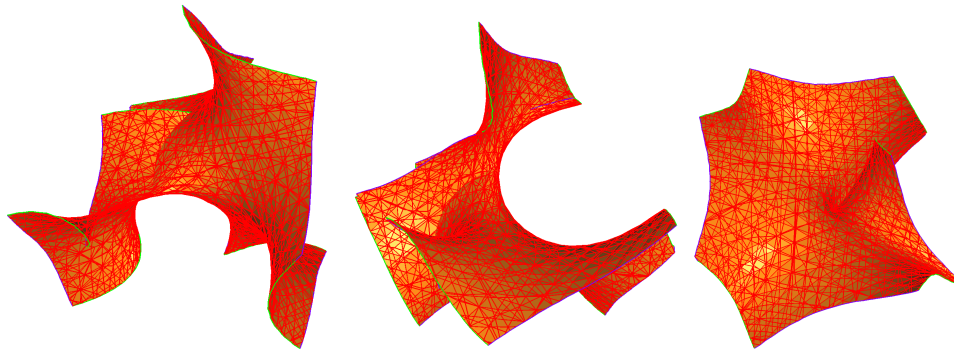
432 **4.3 An application in algebraic geometry**

433 We also applied our algorithm to a more complicated example of interest in algebraic
 434 geometry [4] where an active field of research is to understand the geometry and topology
 435 of various projective varieties. Projective varieties are isomanifolds defined by polynomial
 436 equations in the complex projective space $\mathbb{C}\mathbb{P}^d = (\mathbb{C}^{d+1} \setminus 0) / \mathbb{C}^*$ of complex dimension d .
 437 One such example is the complex one-dimensional curve (that is a real dimensional surface)
 438 given by the equation $z_1^2 \bar{z}_2 + z_2^2 \bar{z}_3 + z_3^2 \bar{z}_1 = 0$ in $\mathbb{C}\mathbb{P}^2$, where \bar{z} denotes the conjugate of the
 439 complex number z .

440 To be able to apply our algorithm, we first need to pass from homogenous coordinates
 441 $[z_1 : \dots : z_{d+1}]$ on \mathbb{CP}^d to affine coordinates $[z'_1 : \dots : z'_{i-1} : 1 : z'_{i+1} : \dots : z'_{d+1}]$ by picking
 442 the i th coordinate to be equal to 1, that is $z'_j = z_j/z_i$. Given some homogenous coordinates
 443 $[z_1 : \dots : z_{d+1}]$, we can choose the i th coordinate to be set to 1 to be the coordinate whose
 444 absolute value is the largest, so that \mathbb{CP}^d can be written as the union of the $d + 1$ sets
 445 $\{[z'_1 : \dots : z'_{i-1} : 1 : z'_{i+1} : \dots : z'_{d+1}] \mid |z'_j| \leq 1\}$, with the boundaries of these sets identified.
 446 Writing $z'_j = x_j + iy_j$ these sets are (seen as real sets) identical to the domain of \mathbb{R}^{2d}

447
$$D_i = \{(x_1, y_1, \dots, x_{i-1}, y_{i-1}, x_{i+1}, y_{i+1}, \dots, x_{d+1}, y_{d+1}) \mid x_j^2 + y_j^2 \leq 1\}.$$

448 Let f be a homogenous polynomial in $d + 1$ complex variables and their complex conjugates.
 449 For each i , we can fix the i th coordinate to be 1. Writing each variable in terms of its real
 450 and imaginary part yields a real inhomogeneous polynomial in $2d$ (real) variables on the
 451 domain D_i . Taking the real and imaginary parts of the function yields two real functions
 452 $f_{\Re,i}$ and $f_{\Im,i}$ on D_i . As real sets, the projective variety $f = 0$ on \mathbb{CP}^d and the intersection
 453 of the sets $f_{\Re,i} = 0$ and $f_{\Im,i} = 0$ on D_i for each i (with the boundaries identified) are the
 454 same. We can therefore apply the tracing algorithm to each isomanifold ($f_{\Re,i} = 0, f_{\Im,i} = 0$)
 455 of D_i independently. Since their boundaries coincide, we can then glue these isomanifolds
 456 along their boundary to obtain a PL-approximation of the projective variety $f = 0$. This, for
 457 example, allows to recover the Euler characteristic of $f = 0$ on \mathbb{CP}^d .
 458 This principle generalizes to varieties of higher codimension, that is to varieties defined by a
 459 number of homogenous polynomials f_1, \dots, f_{d-m} .



460 ■ **Figure 6** The three triangulated surfaces as discussed in the example of $z_1^2 \bar{z}_2 + z_2^2 \bar{z}_3 + z_3^2 \bar{z}_1 = 0$
 461 in \mathbb{CP}^2 after projection from \mathbb{R}^4 to \mathbb{R}^3 .

462 We illustrate the above construction on the above equation $z_1^2 \bar{z}_2 + z_2^2 \bar{z}_3 + z_3^2 \bar{z}_1 = 0$ in \mathbb{CP}^2 .
 463 By passing to affine coordinates, we recover $z_1^2 \bar{z}_2 + z_2^2 + \bar{z}_1 = 0$, $z_1^2 + \bar{z}_3 + z_3^2 \bar{z}_1 = 0$, and
 464 $\bar{z}_2 + z_2^2 \bar{z}_3 + z_3^2 = 0$. By expanding $z_1 = x_1 + iy_1$, $z_2 = x_2 + iy_2$, and $z_3 = x_3 + iy_3$, we find two real
 465 equations for each of the complex equations. We give those corresponding to $z_1^2 \bar{z}_2 + z_2^2 + \bar{z}_1 = 0$,
 466 the other equations being symmetric. For this complex equation, we get the real equations
 467 $x_1 + x_1^2 x_2 + x_2^2 - x_2 y_1^2 + 2x_1 y_1 y_2 - y_2^2 = 0$ and $-y_1 + 2x_1 x_2 y_1 - x_1^2 y_2 + 2x_2 y_2 + y_1^2 y_2 = 0$ in
 468 \mathbb{R}^4 . The domain D_3 is in this case determined by the equations $x_1^2 + y_1^2 \leq 1$ and $x_2^2 + y_2^2 \leq 1$.
 469 Hence we find a surface in \mathbb{R}^4 with a piecewise smooth boundary. The result provided by
 470 our algorithm is shown in Figure 6. For visualization purposes, we show the three surfaces
 471 separately and projected from \mathbb{R}^4 to \mathbb{R}^3 .

472 **5 Conclusion and open questions**

473 We have presented an efficient, practical and provably correct algorithm to compute the
 474 PL-approximation of an isomanifold of any dimension and codimension. Since isomanifolds
 475 are a special type of manifolds, it is tempting to see if our algorithm extends to general
 476 smooth submanifolds of \mathbb{R}^d .

477 The manifold tracing algorithm itself is quite general and works for any submanifold as soon
 478 as we provide a seed point and an oracle that can determine whether a k -simplex of the
 479 ambient triangulation intersects \mathcal{M} or not. In this general setting, the simple algorithm
 480 described above is sufficient to compute a PL-approximation of the manifold and satisfies
 481 the bounds given in Section 3.

482 However, this is not enough to obtain guarantees on the geometric and topological quality
 483 of the output mesh. Such guarantees can be obtained by slightly perturbing the ambient
 484 Coxeter triangulation of type \tilde{A}_d so that the following conditions are satisfied:

- 485 1. All k -dimensional faces τ in \mathcal{T} , with $k \leq d - n - 1$, are far enough from \mathcal{M} .
- 486 2. The longest edge length of \mathcal{T} is upper bounded and its smallest thickness is lower bounded.

487 Under these conditions, Algorithm 1 will output a PL-approximation that is topologically
 488 equivalent and close in Hausdorff distance to the input manifold [10]. However, the
 489 perturbation scheme of [10] perturbs (in the worst case) all the simplices of \mathcal{T} of dimension
 490 less than the codimension $d - n$ that are incident on a vertex (in a neighbourhood of \mathcal{M}).
 491 Since there are exponentially many such simplices, such methods have a complexity that
 492 depends exponentially on the ambient dimension d , and have not proved useful in practice
 493 except in some simple cases. It remains open whether general smooth manifolds embedded
 494 in \mathbb{R}^d can be triangulated in time polynomial in d as we were able to do here in the special
 495 case of isomanifolds.

496

References

- 497 1 Eugene Allgower and Kurt Georg. Estimates for piecewise linear approximations of implicitly
498 defined manifolds. *Applied Mathematics Letters*, 2(2):111–115, 1989.
- 499 2 Eugene Allgower and Kurt Georg. *Numerical continuation methods: an introduction*, volume 13.
500 Springer Science & Business Media, 1990.
- 501 3 Eugene Allgower and Phillip H. Schmidt. An algorithm for piecewise-linear approximation of
502 an implicitly defined manifold. *SIAM Journal on Numerical Analysis*, 22(2):322–346, 1985.
- 503 4 Aurélien Alvarez and Bertrand Deroin. Dynamique et topologie du feuilletage de Jouanolou.
504 Preprint, 2019.
- 505 5 M. A. Armstrong. *Groups and Symmetry*. Springer, 1988.
- 506 6 Dominique Attali, André Lieutier, and David Salinas. Efficient data structure for repre-
507 senting and simplifying simplicial complexes in high dimensions. *International Journal of*
508 *Computational Geometry & Applications*, 22(04):279–303, 2012.
- 509 7 Tom F Banchoff and Wolfgang Kühnel. Equilibrium triangulations of the complex projective
510 plane. *Geometriae Dedicata*, 44(3):313–333, 1992.
- 511 8 Jean-Daniel Boissonnat, Frédéric Chazal, and Mariette Yvinec. *Geometric and Topological*
512 *Inference*. Cambridge Texts in Applied Mathematics. Cambridge University Press, 2018.
513 doi:10.1017/9781108297806.
- 514 9 Jean-Daniel Boissonnat and Arijit Ghosh. Manifold reconstruction using tangential Delaunay
515 complexes. *Discrete & Computational Geometry*, 51(1):221–267, 2014.
- 516 10 Jean-Daniel Boissonnat, Siargey Kachanovich, and Mathijs Wintraecken. Triangulating
517 submanifolds: An elementary and quantified version of whitney’s method. *Discrete & Compu-*
518 *tational Geometry*, pages 1–49, 2020.
- 519 11 Jean-Daniel Boissonnat, CS Karthik, and Sébastien Tavenas. Building efficient and compact
520 data structures for simplicial complexes. *Algorithmica*, 79(2):530–567, 2017.
- 521 12 Jean-Daniel Boissonnat and Clément Maria. The simplex tree: An efficient data structure
522 for general simplicial complexes. *Algorithmica*, 70(3):406–427, 2014. doi:10.1007/
523 s00453-014-9887-3.
- 524 13 Jean-Daniel Boissonnat and Mathijs Wintraecken. The topological correctness of PL-
525 approximations of isomanifolds. In *34th International Symposium on Computational Ge-*
526 *ometry, SoCG 2020, June 23-26, 2020, Zurich, Switzerland.*, 2020. Full version. URL:
527 <https://hal.inria.fr/hal-02386193>.
- 528 14 Jean-Daniel Boissonnat and Mariette Yvinec. *Algorithmic Geometry*. Cambridge Texts in
529 Applied Mathematics. Cambridge University Press, 1998.
- 530 15 Nicolas Bourbaki. Lie groups and Lie algebras. Chapters 4–6. Translated from the 1968 French
531 original by Andrew Pressley. *Elements of Mathematics*, 2002.
- 532 16 Yen-Chi Chen. Solution manifold and its statistical applications, 2020. arXiv:2002.05297.
533 arXiv:2002.05297.
- 534 17 Siu-Wing Cheng, Tamal K Dey, and Edgar A Ramos. Manifold reconstruction from point
535 samples. In *SODA*, pages 1018–1027, 2005.
- 536 18 Aruni Choudhary, Siargey Kachanovich, and Mathijs Wintraecken. Coxeter triangulations
537 have good quality. *Mathematics in Computer Science*, 14:141–176, 2020. URL: <https://doi.org/10.1007/s11786-020-00461-5>.
- 538 19 Aruni Choudhary, Michael Kerber, and Sharath Raghvendra. Polynomial-sized topological
539 approximations using the permutahedron. In Sándor P. Fekete and Anna Lubiw, editors, *32nd*
540 *International Symposium on Computational Geometry, SoCG 2016, June 14-18, 2016, Boston,*
541 *MA, USA*, volume 51 of *LIPICs*, pages 31:1–31:16. Schloss Dagstuhl - Leibniz-Zentrum für
542 Informatik, 2016. doi:10.4230/LIPICs.SoCG.2016.31.
- 543 20 Kenneth L. Clarkson. Tighter bounds for random projections of manifolds. In *Proceedings of*
544 *the 24th ACM Symposium on Computational Geometry, College Park, MD, USA, June 9-11,*
545 *2008*, pages 39–48, 2008. doi:10.1145/1377676.1377685.
- 546

- 547 21 J. H. Conway and N. J. A. Sloane. *Sphere-packings, Lattices, and Groups*. Springer-Verlag
548 New York, Inc., New York, NY, USA, 1987.
- 549 22 Harold S. M. Coxeter. Discrete groups generated by reflections. *Annals of Mathematics*, pages
550 588–621, 1934.
- 551 23 David P. Dobkin, Allan R. Wilks, Silvio V. F. Levy, and William P. Thurston. Contour tracing
552 by piecewise linear approximations. *ACM Transactions on Graphics (TOG)*, 9(4):389–423,
553 1990.
- 554 24 J. J. Duistermaat and J. A. C. Kolk. *Multidimensional Real Analysis I: Differentiation*.
555 Number 86 in Cambridge Studies in Advanced Mathematics. Cambridge University Press,
556 2004.
- 557 25 B. Curtis Eaves. *A course in triangulations for solving equations with deformations*, volume
558 234. Lecture Notes in Economics and Mathematical Systems, 1984.
- 559 26 Armin Eftekhari and Michael B. Wakin. What happens to a manifold under a bi-Lipschitz map?
560 *Discrete & Computational Geometry*, 57(3):641–673, 2017. doi:10.1007/s00454-016-9847-6.
- 561 27 Gideon Ehrlich. Loopless algorithms for generating permutations, combinations, and other
562 combinatorial configurations. *Journal of the ACM (JACM)*, 20(3):500–513, 1973.
- 563 28 Hans Freudenthal. Simplicialzerlegungen von beschränkter flachheit. *Annals of Mathematics*,
564 pages 580–582, 1942.
- 565 29 A. Gomes, I. Voiculescu, J. Jorge, B. Wyvill, and C. Galbraith. *Implicit Curves and Surfaces:*
566 *Mathematics, Data Structures and Algorithms*. Springer, 2009.
- 567 30 GUDHI Project. URL: <http://gudhi.gforge.inria.fr/doc/latest/>.
- 568 31 James E. Humphreys. *Reflection groups and Coxeter groups*, volume 29. Cambridge university
569 press, 1992.
- 570 32 Siargey Kachanovich. *Meshing submanifolds using Coxeter triangulations*. Theses, COMUE Uni-
571 versité Côte d’Azur (2015 - 2019), October 2019. URL: <https://hal.inria.fr/tel-02419148>.
- 572 33 William E. Lorensen and Harvey E. Cline. Marching cubes: A high resolution 3d surface
573 construction algorithm. *ACM siggraph computer graphics*, 21(4):163–169, 1987.
- 574 34 M. Maes and B. Kappen. On the permutahedron and the quadratic placement problem. *Philips*
575 *Journal of Research*, 46(6):267–292, 1992.
- 576 35 Chohong Min. Simplicial isosurfacing in arbitrary dimension and codimension. *Journal of*
577 *Computational Physics*, 190(1):295–310, 2003.
- 578 36 Timothy S. Newman and Hong Yi. A survey of the marching cubes algorithm. *Computers &*
579 *Graphics*, 30(5):854 – 879, 2006. URL: <http://www.sciencedirect.com/science/article/pii/S0097849306001336>, doi:<https://doi.org/10.1016/j.cag.2006.07.021>.
- 580 37 James M Ortega and Werner C Rheinboldt. *Iterative solution of nonlinear equations in several*
581 *variables*. SIAM, 2000.
- 582 38 Alexander M Ostrowski. *Solution of Equations and Systems of Equations: Pure and Applied*
583 *Mathematics: A Series of Monographs and Textbooks, Vol. 9*, volume 9. Elsevier, 2016.
- 584 39 B.C. Rennie and A.J. Dobson. On Stirling numbers of the second kind. *Journal of Combinatorial*
585 *Theory*, 7(2):116 – 121, 1969. doi:[https://doi.org/10.1016/S0021-9800\(69\)80045-1](https://doi.org/10.1016/S0021-9800(69)80045-1).
- 586 40 Frank Ruskey and Carla D. Savage. Gray codes for set partitions and restricted growth tails.
587 *Australasian J. Combinatorics*, 10:85–96, 1994.
- 588 41 Michael J. Todd. *The computation of fixed points and applications*, volume 124. Lecture Notes
589 in Economics and Mathematical Systems, 1976.
- 590 42 Nakul Verma. A note on random projections for preserving paths on a manifold. Technical
591 Report Tech. Report CS2011-0971, UC San Diego, 2011.
- 592 43 Timothy R. Walsh. Loop-free sequencing of bounded integer compositions. *Journal of*
593 *Combinatorial Mathematics and Combinatorial Computing*, 33:323–345, 2000.
- 594 44 Rephael Wenger. *Isosurfaces: geometry, topology, and algorithms*. AK Peters/CRC Press,
595 2013.
- 596 45 H. Whitney. *Geometric Integration Theory*. Princeton University Press, 1957.

- 598 46 G. M. Ziegler. *Lectures on Polytopes*. Graduate Texts in Mathematics. Springer New York,
599 2012. URL: <https://books.google.fr/books?id=xd25TXSSUcgC>.

600 **A** A compact data structure for high-dimensional
 601 Coxeter-Freudenthal-Kuhn triangulations

602 Subdivisions of Euclidean space are a major tool to efficiently answer geometric queries,
 603 compute approximation of shapes or solve optimization problems. Among the most widely
 604 used subdivision schemes are grids and triangulations. Both are subject to the curse of
 605 dimensionality and their combinatorial complexity depends exponentially on the dimension
 606 of the space. Triangulations are most flexible since their vertex set can be any set of points.
 607 Differently, uniform grids depend only on the space but not on a given data set. The rigidity
 608 of the grid structure has a major advantage: the grid, although of exponential size, need not
 609 be represented explicitly and basic operations like locating a point or computing faces or
 610 cofaces of a given cell in the grid can be done without storing an explicit representation of
 611 the grid. In fact, the representation can be entirely implicit. This is clearly impossible with
 612 general triangulations with arbitrary vertex sets.

613 The question of designing efficient data structure for triangulations and more general simplicial
 614 complexes led to interesting developments recently. On one hand, one can take advantage
 615 of the fact that special types of simplicial complexes allow compact representations. Most
 616 notably, flag complexes (including the celebrated Vietoris-Rips complex) can be represented
 617 by their 1-skeleton (or graph) and higher dimensional faces can be retrieved by computing
 618 the cliques of the graph. One can also represent a simplicial complex by its blockers, i.e. the
 619 simplices that do not belong to the complex but whose facets do [6].

620 On a different front, data structures have been proposed to efficiently store general simplicial
 621 complexes such as the simplex tree [12] that uses a trie to store the faces of all dimensions,
 622 or the Simplex Array List [11] that represents only the maximal faces, which allows an
 623 exponential saving in storage since a simplex has exponential complexity. Nevertheless, due
 624 to their generality and the fact that the represented complexes don't have any prespecified
 625 symmetry, the data structures cannot compete with grids in terms of size and efficiency.

626 The Coxeter-Freudenthal-Kuhn triangulations in this paper form a middle ground, they form
 627 a special class of triangulations of \mathbb{R}^d that have a high regularity. The data structure for
 628 such triangulations that can be as compact as for grids.

629 The Coxeter-Freudenthal-Kuhn triangulations we consider combine two classes of triangula-
 630 tions with different origins and names. The two foundational works are due to Coxeter [22]
 631 and Freudenthal [28]. Coxeter triangulations derive from geometric group theory, in particu-
 632 lar affine Weyl groups, while Freudenthal triangulations (also called Kuhn triangulations)
 633 are combinatorial in nature. Nevertheless, both triangulations are the same up to a linear
 634 transformation, as remarked in [23] and fully proved in this paper. This allows us to combine
 635 the nice geometric properties of Coxeter triangulations of type \tilde{A}_d with the simple combina-
 636 torial definitions of the Freudenthal-Kuhn triangulation, and its connection to permutahedra.
 637 Coxeter triangulations of type \tilde{A}_d are geometrically attractive because each simplex is very
 638 well shaped (large volume compared to longest edge length), and all d -simplices are identical
 639 up to reflections.

640 Although these triangulations do not depend on a given data set, they proved to be very
 641 useful in to interpolate multivariate multivalued functions or to mesh geometric shapes
 642 embedded in high dimensional spaces. Freudenthal-Kuhn triangulations have been known in
 643 Applied Mathematics [2, 25, 41], and Coxeter triangulations have been used by Dobkin et
 644 al. [23] to trace curves in high dimensions and are good candidates to trace manifolds of any
 645 codimension [35]. They have also been used in the context of Topological Data Analysis [19].
 646 In Appendix A.1, we study these triangulations. This section recalls and extends to arbitrary

647 dimensions several results that were disseminated in many different places which are sometimes
 648 difficult to access and in different languages (see among others [28, 41, 25, 34, 46, 39, 23]).
 649 Based on these results, we introduce in Appendix A.2 a very compact data structure that
 650 implicitly stores the full facial structure of such triangulations. The data structure allows to
 651 locate a point in the triangulation and to retrieve the faces or the cofaces of a simplex of any
 652 dimension in an output sensitive way.

653 The Data Structure has been implemented and fully tested. Section 4 reports on experi-
 654 mental results and demonstrates that the data structure is highly practical and can handle
 655 triangulations of high dimensional spaces. Using our data structure will allow to extend the
 656 applicability of the methods based on such triangulations and to significantly improve their
 657 performance. It appears to be especially useful to trace low dimensional manifolds embedded
 658 in high dimensional spaces as encountered in statistics, dynamical systems, econometrics, or
 659 mechanics [16, 41, 36].

660 A.1 Coxeter-Freudenthal-Kuhn triangulations

661 Freudenthal-Kuhn triangulations are combinatorial structures that come from a specific
 662 triangulation of the d -cube. Their connections to permutahedra is at the heart of our data
 663 structure. Coxeter triangulations, we introduce in Section A.1.3, have a different flavour
 664 and come with very nice geometric properties. Since both types of triangulations are the
 665 same up to an affine transformation, as first noted by Dobkin et al [23], they have the same
 666 combinatorial structure and our data structure will be able to handle both of them.
 667 Although most ideas in this section were known previously, we give full proofs of the results
 668 that were not explicitly mentioned or not proved in full generality in the literature.

669 A.1.1 Permutahedra

670 We write $[i] = \{1, \dots, i\}$, and $[i, j] = \{i, \dots, j\}$.

671 ► **Definition 14** (Permutahedron). *A d -permutahedron is a d -dimensional polytope, which is*
 672 *the convex hull \mathcal{P} of all points in \mathbb{R}^{d+1} , the coordinates of which are permutations of $[d + 1]$.*
 673 *Formally, this convex hull can be written as:*

$$674 \quad \mathcal{P} = \text{conv}\{(\sigma(1), \dots, \sigma(d + 1)) \in \mathbb{R}^{d+1} \mid \sigma \in \mathfrak{S}_{d+1}\},$$

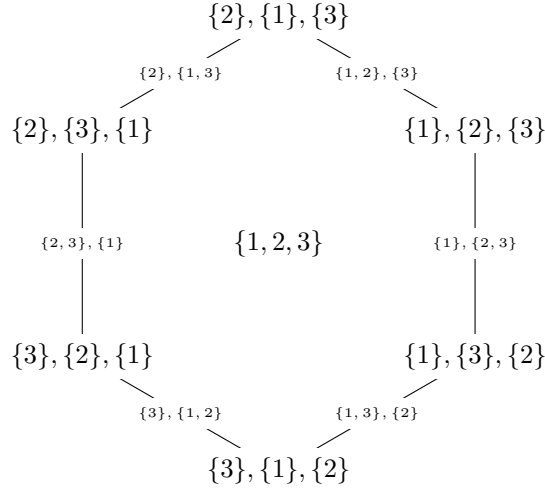
675 where \mathfrak{S}_{d+1} denotes the set of permutations of $[d + 1]$. If there is a need to distinguish
 676 permutahedra of different dimension we write $\mathcal{P}(n)$ the permutahedron of dimension $n - 1$.

677 \mathcal{P} is at most d -dimensional since all its vertices lie on the hyperplane of equation

$$678 \quad \sum_{i=1}^{d+1} x^i = \frac{d(d + 1)}{2}.$$

679 Moreover, it can be shown that there are $d + 1$ affinely independent vertices in \mathcal{P} , proving
 680 that \mathcal{P} is exactly d -dimensional (see for example [34, Lemma 3.4]). The facial structure of \mathcal{P}
 681 is best described in terms of ordered partitions [46]. Refer to Figure 7.

683 ► **Definition 15** (Ordered partition). *Let T be a finite non-empty set, $|T|$ its cardinality, and*
 684 *$l \leq |T|$ a positive integer. An ordered partition of T in l parts is a collection of l indexed*
 685 *subsets $\omega = (\omega_1, \dots, \omega_l)$, such that $\omega_i \subseteq T$, and $\{\omega_1, \dots, \omega_l\}$ is a partition of T . The ω_i*
 686 *are called the parts and are ordered by their index. We write $OP_l[d]$ for the set of ordered*
 687 *partitions of $[d]$ with l parts, and just $OP[d]$ for the set of all ordered partitions of $[d]$.*



682 **Figure 7** The 2-permutahedron and the ordered partitions associated to its faces.

688 **Definition 16 (Refinement).** Let ω , and ϖ be two ordered partitions of $[d + 1]$ in l , and p
 689 parts respectively, with $1 \leq l \leq p \leq d + 1$. We say that ϖ is a refinement of ω if there exist
 690 positive integers a_1, \dots, a_l , such that

- 691 \blacksquare $(\varpi_1, \dots, \varpi_{a_1})$ is an ordered partition of ω_1 in a_1 parts,
- 692 \blacksquare $(\varpi_{a_1+1}, \dots, \varpi_{a_1+a_2})$ is an ordered partition of ω_2 in a_2 parts,
- 693 \blacksquare \dots ,
- 694 \blacksquare $(\varpi_{a_1+\dots+a_{l-1}+1}, \dots, \varpi_{a_1+\dots+a_l})$ is an ordered partition of ω_l in a_l parts.

695 We recall Theorem 3.6 of [34]:

696 **Lemma 17 (Facial structure of the permutahedron).** The faces of a d -permutahedron are in
 697 bijection with the ordered partitions of $[d + 1]$. More precisely, the i -faces of \mathcal{P} correspond to
 698 ordered partitions of $[d + 1]$ into $l = d + 1 - i$ parts $(\omega_1, \dots, \omega_l)$. If σ , and τ are two faces of
 699 a d -permutahedron, σ is a subface of τ (denoted $\sigma \subseteq \tau$) if and only if the ordered partition
 700 associated to σ is a refinement of the ordered partition associated to τ .

701 We also need the following result from [34, Corollary 3.15], and [39, Theorem 3].

702 **Corollary 18.** The number of $(d - i)$ -dimensional faces in a d -permutahedron is $(i +$
 703 $1)! S(d + 1, i + 1)$, where $S(\cdot, \cdot)$ is the Stirling number of the second kind. It is bounded by
 704 $2^{2(d+1) \log(i+1)}$.

705 The following three corollaries seem to be new.

706 **Corollary 19.** The number $p_{0,i}$ of vertices of a i -face of a d -permutahedron is at most
 707 $(i + 1)!$, and at least $2^{\min(i, d-i)}$.

708 The proof of Corollary 19 is based on:

709 **Lemma 20 (Lemma 3.11 of [34]).** The face of a permutahedron corresponding to an ordered
 710 partition $\omega = (\omega_1, \dots, \omega_{l+1})$ is combinatorially

711
$$\mathcal{P}(|\omega_1|) \times \dots \times \mathcal{P}(|\omega_{l+1}|),$$

712 where $|\omega_p|$ denotes the length of the p -th part of the ordered partition, and $\mathcal{P}(n)$ the permuta-
 713 hedron of dimension $n - 1$.

714 **Proof of Corollary 19.** Write $l = d - i$. Since the number of vertices of the product of two
 715 polytopes is the product of the vertices, and a $(n - 1)$ -dimensional permutahedron has $n!$
 716 vertices, we see that the total number of vertices of a i -face of a d -dimensional permutahedron
 717 corresponding to an ordered partition $\omega = (\omega_1, \dots, \omega_{l+1})$ is

$$718 \quad \prod_{p=1}^{l+1} (|\omega_p|!).$$

719 Let $1 \leq j < k \leq d$ be integers such that $j + k = d + 1$. By definition $j!k! < (j - 1)!(k + 1)!$,
 720 and thus $j!k! \leq 1!d!$. Generalizing this, we see that the product of the $|\omega_p|!$ is maximal when
 721 all parts are singletons except the biggest part which has $d + 1 - l$ elements. Therefore

$$722 \quad \prod_{p=1}^{l+1} (|\omega_p|!) \leq (d - l + 1)!.$$

723 Using the inverse argument, the lower bound is obtained when each part in the ordered
 724 partition are as small as possible that is all parts have almost equal size. In this case,
 725 $|\omega_p| \geq \lfloor \frac{d+1}{l+1} \rfloor$, so that

$$726 \quad \prod_{p=1}^{l+1} (|\omega_p|!) \geq \left(\left\lfloor \frac{d+1}{l+1} \right\rfloor! \right)^{l+1}$$

727 More accurately, let r' be the remainder of $d + 1$ after division by $l + 1$, that is $r' = d + 1$
 728 $\text{mod } l + 1$ then:

$$729 \quad \prod_{p=1}^{l+1} (|\omega_p|!) \geq \left(\left\lfloor \frac{d+1}{l+1} \right\rfloor! \right)^{l-r'+1} \left(\left(\left\lfloor \frac{d+1}{l+1} \right\rfloor + 1 \right)! \right)^{r'}$$

730 We now distinguish two cases:

731 ■ If $\lfloor \frac{d+1}{l+1} \rfloor \geq 2$, and thus $\frac{d+1}{2} \geq l + 1$, then we see that

$$732 \quad \prod_{p=1}^{l+1} (|\omega_p|!) \geq 2^{l+1}.$$

733 ■ If $\lfloor \frac{d+1}{l+1} \rfloor = 1$, we have that $\frac{d+1}{2} < l + 1 \leq d + 1$, and thus $r' = d + 1 \text{ mod } l + 1 = d - l$.
 734 Hence,

$$735 \quad \prod_{p=1}^{l+1} (|\omega_p|!) \geq 2^{d-l}.$$

736 Because $l + 1 = d - l$, or $2l + 1 = d$ is precisely the point where you go from the first to the
 737 second case we see that

$$738 \quad \prod_{p=1}^{l+1} (|\omega_p|!) \geq 2^{\min\{l+1, d-l\}}$$

739



740 ► **Corollary 21.** *The number of facets of an i -face σ of a d -permutahedron is at most 2^{i+1} .*

XX:24 Isomanifold Tracing in \mathbb{R}^d , using Coxeter-Freudenthal-Kuhn Triangulations

741 **Proof.** Write $l = d - i$. We first recall a set of $d > 2$ objects can be subdivided in two
 742 non-empty ordered subsets A and B in $2^d - 2$ ways. This is not hard to see. Because we
 743 pick for each element if it will be put in A or B there are 2^d possibilities. Excluding that A
 744 or B is empty gives $2^d - 2$. Let $\omega = (\omega_1, \dots, \omega_l)$ again be an ordered partition. To find a
 745 refinement of ω in $l + 1$ parts, we need to first pick a $1 \leq p \leq l$, such that $|\omega_p| > 1$, and then
 746 we need to break ω_p up into two (ordered) parts, for which there are $2^{|\omega_p|} - 2$ possibilities
 747 as we have seen above. This means that if $I = \{p \mid 1 \leq p \leq l, |\omega_p| > 1\}$, the number of
 748 refinements is

$$749 \quad \sum_{p \in I} 2^{|\omega_p|} - 2.$$

750 Let now $1 \leq s < t \leq d$ be integers such that $s + t = d + 1$. Then $2^s + 2^t < 2^{s-1} + 2^{t+1}$.
 751 Generalizing this, we see that the sum of the $2^{|\omega_p|} - 2$ is maximal when all $|\omega_p| = 1$ except
 752 the biggest part which has $d - l + 1 = i + 1$ elements. ◀

753 ▶ **Corollary 22.** Let $p_{i,j}$ denote the number of i -faces of a j -face of the d -permutahedron.
 754 We have

$$755 \quad p_{i,j} \leq \frac{1}{2^{\min(i,d-i)}} \binom{j}{i} (j + 1)!$$

756

757 Corollary 22 generalizes the previous two corollaries. For $i = 0$, the bound in Corollary 22 is
 758 the same as the upper bound in Corollary 19. For $i = j - 1$, the bound is comparable but
 759 weaker than the bound in Corollary 21.

760 **Proof of Corollary 22.** Let σ be a j -face of the d -permutahedron. Write $F_{i,\sigma}$ for the set of
 761 i -faces of σ , and c_v for the number of i -cofaces of a vertex v of σ , i.e. the number of simplices
 762 of $F_{i,\sigma}$ that contain v . For $\tau \in F_{i,\sigma}$, we write p_τ for the number of vertices of τ . By double
 763 counting the incidences between vertices, and i -faces inside σ , we have

$$764 \quad \sum_{\tau \in F_{i,\sigma}} p_\tau = \sum_{v \in F_{0,\sigma}} c_v.$$

765 Now observe that the d -permutahedron is a simple polytope (this follows from the fact that
 766 its dual is simplicial since it is a star in the FK-triangulation). The faces of simple polytopes
 767 are also simple polytopes which implies that the vertices of a j -face are incident to $\binom{j}{i}$ faces
 768 of dimension i [14, Lemma 7.1.14]. Moreover, $|F_{0,\sigma}| \leq (j + 1)!$ by Corollary 19. Hence

$$769 \quad \sum_{v \in F_{0,\sigma}} c_v = \binom{j}{i} |F_{0,\sigma}| \leq \binom{j}{i} (j + 1)!$$

770 In addition, by Corollary 19, we have

$$771 \quad \sum_{\tau \in F_{i,\sigma}} p_\tau \geq 2^{\min(i,d-i)} |F_{i,\sigma}|$$

772 The inequality follows since σ is any j -face of the d -permutahedron. ◀

773 **A.1.2 Freudenthal-Kuhn triangulation**

774 The Freudenthal-Kuhn (FK for short) triangulation is obtained from the d -grid, i.e. the
 775 unit cubical tessellation of \mathbb{R}^d that consists of copies of the unit d -cube along the integer
 776 lattice \mathbb{Z}^d . By triangulating each d -cube in the grid in an appropriate way to be described
 777 now, we obtain the FK-triangulation of \mathbb{R}^d . The results and definitions below were known
 778 to Freudenthal [28], Todd [41], or Eaves [25], mainly for top dimensional simplices and in
 779 different guises. We combine these results and extend to simplices of arbitrary (co)dimension,
 780 where necessary.

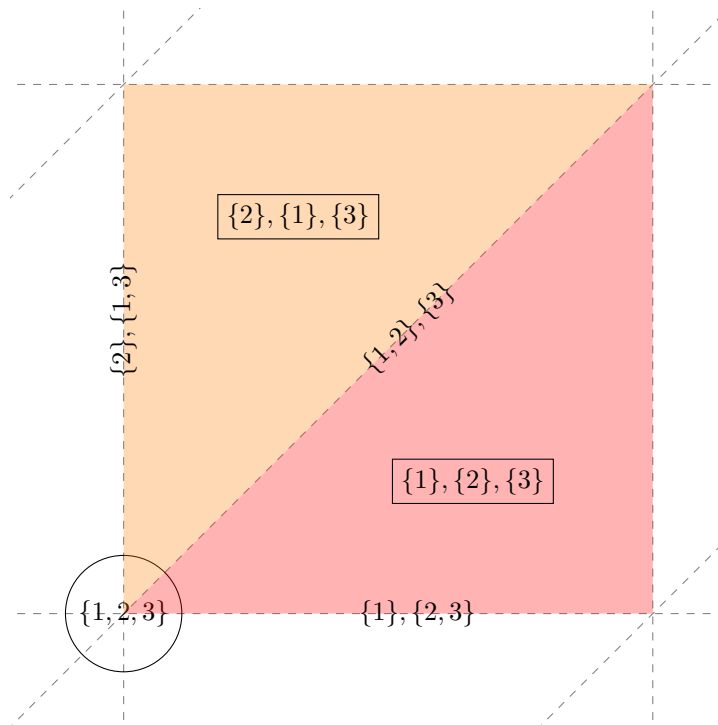
781 ► **Definition 23.** Let $x \in \mathbb{R}^d$, and write $z^i = x^i - \lfloor x^i \rfloor$. We denote by e_1, \dots, e_d the basis
 782 vectors and introduce, for reasons that will be clear later, the extra vector

783
$$e_{d+1} = - \sum_{i=1}^d e_i.$$

784 We introduce the convention that $z^{d+1} = 0$. We associate to x the ordered partition $\omega =$
 785 $(\omega_1, \dots, \omega_{l+1})$ of $[d + 1]$ where the ω_i are obtained by sorting the z^i in decreasing order.
 786 Specifically, with $\omega_i = \{\omega_i(1), \dots, \omega_i(m_i)\}$, we have (see Figure 8):

787
$$1 > z^{\omega_1(1)} = \dots = z^{\omega_1(m_1)} > \dots > z^{\omega_l(1)} = \dots = z^{\omega_l(m_l)}$$

 788
$$> z^{\omega_{l+1}(1)} = \dots = z^{\omega_{l+1}(m_{l+1})} = 0. \tag{2}$$



789 ■ **Figure 8** The ordered partitions associated to the faces of the FK-triangulation of \mathbb{R}^2 that have
 790 the same minimal vertex v_0 (circled).

791 **► Lemma 24.** Suppose that $\omega = (\omega_1, \dots, \omega_{l+1})$ is an ordered partition of $[d+1]$ such that
 792 $d+1 \in \omega_{l+1}$, and let $\sigma = \{v_0, \dots, v_l\}$ be the l -simplex whose vertices are the points

$$793 \quad v_0 = (\lfloor x^1 \rfloor, \dots, \lfloor x^d \rfloor), \quad v_i = v_{i-1} + \sum_{j \in \omega_i} e_j \quad i = 1, \dots, l. \quad (3)$$

794 Then x is a point in the relative interior of σ if and only if $z^i = x^i - \lfloor x^i \rfloor$, $i = 1, \dots, d+1$
 795 (with, as above, $z^{d+1} = 0$), satisfy (2).

796 **Proof.** Because the whole problem is translation invariant, we assume that $v_0 = 0$ without
 797 loss of generality, so that the expressions are shorter. Using barycentric coordinates, $z \in \sigma$
 798 can be written as

$$799 \quad z = \sum_{i=0}^l \lambda_i v_i = \sum_{i=0}^l \lambda_i \sum_{k=1}^i \sum_{j \in \omega_i} e_j$$

$$800 \quad = \lambda_l \left(\sum_{k \in \omega_l} e_k \right) + (\lambda_l + \lambda_{l-1}) \left(\sum_{k \in \omega_{l-1}} e_k \right) + \dots + (\lambda_l + \dots + \lambda_1) \left(\sum_{k \in \omega_1} e_k \right). \quad (4)$$

801 Here the $\lambda_i > 0$, $i \in [0, l]$, $\sum_{i=0}^l \lambda_i = 1$, are the barycentric coordinates of z in σ . We have

$$802 \quad \alpha_{\omega_l(1)} = \dots = \alpha_{\omega_l(m_l)} = \lambda_l$$

$$803 \quad \quad \quad \vdots$$

$$804 \quad \alpha_{\omega_1(1)} = \dots = \alpha_{\omega_1(m_1)} = \lambda_l + \dots + \lambda_1 \quad (5)$$

805 From (4), we see that $\alpha_{\omega_i(j)}$ is the $\omega_i(j)$ th coordinate of z , denoted by $z^{\omega_i(j)}$, while all
 806 coordinates $z^{\omega_{l+1}(1)}, \dots, z^{\omega_{l+1}(m_{l+1})}$ are zero, because $e_{\omega_{l+1}(i)}$ does not occur in (4), for all i .
 807 Moreover, because $\lambda_l + \dots + \lambda_i > \lambda_l + \dots + \lambda_{i-1}$, we see that (2) is satisfied.
 808 Conversely, given a point z such that its coordinates satisfy (2), we can read of its barycentric
 809 coordinates with respect to the v_i , as defined by (3), from (5). \blacktriangleleft

810 **► Theorem 25.** The equivalence classes of the points of \mathbb{R}^d with a same ordered partition
 811 are the simplices of a triangulation of \mathbb{R}^d called the FK-triangulation (see Figure 8).

812 **Proof.** Lemma 24 implies that:

- 813 \blacksquare Any face of a simplex in the FK-triangulation also lies in the FK-triangulation.
- 814 \blacksquare The intersection of two simplices in the FK-triangulation also lie in the FK-triangulation.
- 815 \blacksquare For any point $x \in \mathbb{R}^d$, there is a unique simplex σ such that x lies in the relative interior
 816 of σ . Indeed, x has uniquely defined barycentric coordinates with respect to the vertices
 817 of σ , and thus is mapped to a unique point in σ .

818 Hence the partition we have defined is a well-defined triangulation of \mathbb{R}^d . \blacktriangleleft

819 **► Remark 26.** We note that, by construction, v_0 in Lemma 24 is the smallest vertex of σ
 820 in the lexicographical order. Lemma 24 also implies an observation of Freudenthal [28]: all
 821 d -simplices in the FK-triangulation can be described by monotone paths along the edges of
 822 the cube from vertex $(0, \dots, 0) + v_0$ to vertex $(1, \dots, 1) + v_0$. Conversely, any monotone path
 823 along the edges of the cubes from $(0, \dots, 0) + v_0$ to $(1, \dots, 1) + v_0$ gives a simplex in the
 824 FK-triangulation.

825 **A.1.3 CFK-triangulations**

826 Freudenthal-Kuhn triangulations are closely related to Coxeter triangulations of type \tilde{A}_d [18]
 827 and both are arrangements of hyperplanes as demonstrated now.

828 Let E be a finite set of vectors of \mathbb{R}^d , and consider the set of hyperplanes $H_E = \{x \in \mathbb{R}^d \mid$
 829 $\langle x, u \rangle = k, u \in E, k \in \mathbb{Z}\}$. In generalization of the theory of Coxeter triangulations, we call
 830 the set E the set of roots for historic reasons, as mentioned below.

831 These hyperplanes partition \mathbb{R}^d in a cell complex called the *arrangement* of the hyperplanes.
 832 We denote it by \mathcal{H}_E .

833 **► Lemma 27.** *The Freudenthal-Kuhn triangulation is the hyperplane arrangement $\mathcal{H}_{E_{FK}}$*
 834 *associated to the set of vectors $E_{FK} = \{e_1, \dots, e_d\} \cup \{u_{i,j} = e_j - e_i \mid 1 \leq i < j \leq d\}$.*

835 **Proof.** Thanks to Lemma 24, we know that if $x \in \sigma$, where σ is a simplex of dimension less
 836 than d , there is at least one equality in (2) on top of $z^{d+1} = 0$. That is $x^i - \tilde{v}_0^i = x^j - \tilde{v}_0^j$ or
 837 $x^i - \tilde{v}_0^i = 0$ for some $i, j \neq d + 1$. Note that $\tilde{v}_0^i, \tilde{v}_0^j \in \mathbb{Z}$. The converse direction of Lemma 24
 838 gives that if $x^i - \tilde{v}_0^i = x^j - \tilde{v}_0^j$ or $x^i - \tilde{v}_0^i = 0$ for some $i, j \neq d + 1$ for $x \in \mathbb{R}^d$, then there is a
 839 simplex σ of dimension strictly less than d in the FK-triangulation such that $x \in \sigma$. ◀

840 Observe that the norms of the vectors in E_{FK} are either 1 or $\sqrt{2}$. By definition, this implies
 841 that the distance between the two hyperplanes $\langle x, u \rangle = k$, and $\langle x, u \rangle = k + 1$, where $u \in E_{FK}$,
 842 is either 1 or $1/\sqrt{2}$.

843 Let H be the hyperplane of \mathbb{R}^{d+1} of equation $\langle x, \mathbf{1} \rangle = 0$ where $\mathbf{1}$ is the vector of \mathbb{R}^{d+1} whose
 844 coordinates are all 1. We now define a linear map μ from \mathbb{R}^d to H by showing how it acts
 845 on the basis of \mathbb{R}^d : $\mu(e_i) = r_{1,i} = \sum_{j=1}^i s_j$, where $s_i = e_i - e_{i+1}$, $i = 1, \dots, d$. The vectors
 846 s_j are called simple roots and play an important role in algebra. We refer to [18] for more
 847 information.

848 **► Lemma 28.** μ maps E_{FK} bijectively onto the set E_C defined as

849
$$E_C = \left\{ r_{i,j} = \sum_{l=i}^j s_l = e_i - e_{j+1} \mid 1 \leq i \leq j \leq d \right\}$$

850 **Proof.** The vector $\mu(e_i) = r_{1,i}$ lies in E_C , by definition. For $u_{i,j} \in E_{FK}$, with $i < j$, we see
 851 that

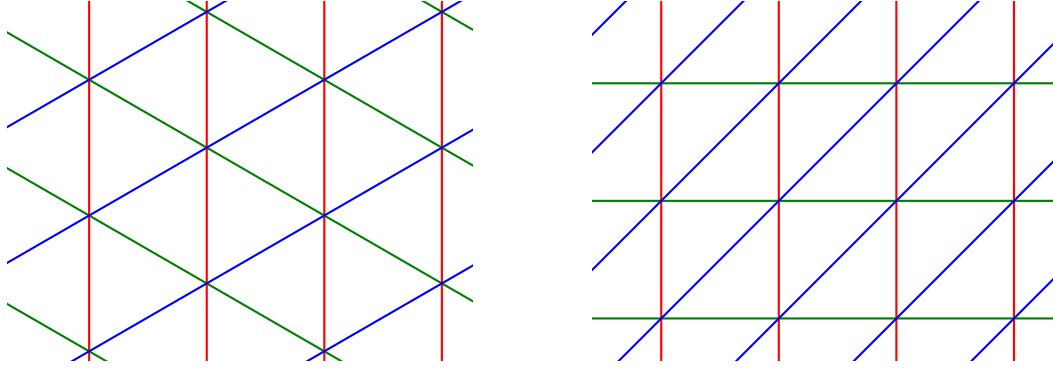
852
$$\mu(u_{i,j}) = \mu(e_j - e_i) = \mu(e_j) - \mu(e_i) = r_{1,j} - r_{1,i} = \sum_{l=1}^j s_l - \sum_{l=1}^i s_l = \sum_{l=i+1}^j s_l = r_{i+1,j}.$$

853 Hence $\mu(u_{i,j})$ lies in E_C . By reading the previous calculation backwards, we see that μ^{-1}
 854 maps each $r \in E_C$ to a vector in E_{FK} . ◀

855 Observe that all vectors in E_C have length $\sqrt{2}$. By definition, this implies that the distance
 856 between the two hyperplanes $\langle x, u \rangle = k$, and $\langle x, u \rangle = k + 1$, where $u \in E_C$, is $1/\sqrt{2}$.

857 The image by μ of the Freudenthal-Kuhn triangulation is a triangulation of \mathbb{R}^d which is
 858 the arrangement \mathcal{H}_{E_C} associated to the set of vectors E_C . This triangulation is called the
 859 *Coxeter triangulation* of type \tilde{A}_d of \mathbb{R}^d . By definition, it has the same combinatorial structure
 860 as the FK-triangulation. In addition, it has remarkable geometric properties [23, 18]. First,
 861 it is a non-degenerate Delaunay triangulation, and its dual complex is a Voronoi diagram.
 862 Moreover, its simplices have an exceptionally large thickness (the ratio of the smallest altitude
 863 of a simplex over its diameter or longest edge length).

864 We will call any triangulation of \mathbb{R}^d that is the image of a Freudenthal-Kuhn triangulation
 865 under a non-degenerate affine map a Coxeter-Freudenthal-Kuhn triangulation, or CFK-
 866 triangulation for short. This includes the Coxeter triangulation of type \tilde{A}_d (as embedded in
 867 \mathbb{R}^d).



868 **Figure 9** The Coxeter and Freudenthal-Kuhn triangulations in the plane.

869 **A.2 Data Structure**

870 We introduce our data structure in this section. We first consider the case of FK-triangulations
 871 in Sections A.2.1 and A.2.2. The extension to CFK-triangulations in Section A.3 is straight-
 872 forward, since all these triangulations have the same combinatorial structure.

873 **A.2.1 Permutahedral representation of FK-triangulations**

874 **Cycles and the permutahedron.** In Remark 26 we have seen that simplices can be described
 875 by monotone paths (increasing coordinates) along the edges of the cube. As observed by Eaves
 876 [25], these monotone paths can be made into a cycle using the extra vector $e_{d+1} = -\sum_{i=1}^d e_i$
 877 because by construction

878
$$v_0 = v_l + \sum_{i \in \omega_{l+1}} e_i,$$

879 with ω as in Definition 23. Because it is a cycle, we can take any vertex of the cycle as a
 880 starting point, which means that v_0 no longer has a special role as a starting point of a
 881 monotone edge walk. A cycle can now be represented by an ordered partition of $[d + 1]$, for
 882 which it is not longer necessary that $d + 1$ lies in ω_{l+1} , and an (arbitrary) starting point. We
 883 now formalize these general cyclical paths:

884 **Definition 29** (Permutahedral representation). *Let $(v_0, \omega) \in \mathbb{Z}^d \times OP_{l+1}[d]$. To this pair*
 885 *we associate a simplex $\sigma^\omega = \{v_0 = v_0^\omega, v_1^\omega, \dots, v_l^\omega\}$ with*

886
$$v_i^\omega = v_{i-1}^\omega + \sum_{i \in \omega_i} e_i \quad i = 1, \dots, l. \tag{6}$$

887 *We say that (v_0, ω) is the permutahedral representation of the simplex σ^ω . If $d + 1 \in \omega_{l+1}$,*
 888 *we say that (v_0, ω) is the canonical permutahedral representation of σ^ω . In this case, σ^ω is*
 889 *a simplex in the FK-triangulation in the cube of which v_0 is the minimal vertex with respect*
 890 *to the lexicographical order, as we have seen above.*

891 In Lemma 32, and Proposition 33, we will see that, more generally, $\{(v_0, \omega) \mid \omega \in OP[d + 1]\}$
 892 is the star of v_0 in the FK-triangulation, where we identify simplices with their permutahedral
 893 representations.

894 ► **Definition 30** (Cyclic shifts). *Let (v_0, ω) be a permutahedral representation. We define the*
 895 *cyclic shift of (v_0, ω) of length k to the left as (v'_0, ω') , where*

$$896 \quad v'_0 = v_0 + \sum_{j=1}^k \sum_{i \in \omega_j} e_i \qquad \omega'_j = \omega_{(j+k-1) \bmod (l+1)+1}. \qquad (7)$$

897 Here we use the convention that the sum from 1 to 0 is empty. We write $(v'_0, \omega') = (v_0, \omega) \oplus k$.

898 ► **Lemma 31.** *The cyclic shift $(v'_0, \omega') = (v_0, \omega) \oplus k$ defines the same simplex as (v_0, ω) .*

899 **Proof.** Follows by inserting (7) in (6). ◀

900 We now prove that the all permutahedral representations for a fixed v_0 , form the star of v_0 .
 901 This is a crucial property that will be used to efficiently compute faces, and cofaces, and
 902 traverse the triangulation.

903 ► **Lemma 32.** *The set $\{(v_0, \omega) \mid \omega \in OP[d + 1]\}$, where $OP[d + 1]$ is the set of all ordered*
 904 *partitions of $[d + 1]$, gives all the simplices in the star of v_0 in FK-triangulation.*

905 **Proof.** Let (v_0, ω) , with $\omega \in OP_{l+1}[d + 1]$, be such that $d + 1 \in \omega_k$. Let $(v'_0, \omega') =$
 906 $(v_0, \omega) \oplus (l - k + 1)$. By Definition 30, and Lemma 31, (v_0, ω) , and (v'_0, ω') represent the same
 907 simplex. Moreover $d + 1 \in \omega'_{l+1}$, that is (v'_0, ω') is a canonical permutahedral representation.
 908 This implies that (v'_0, ω') lies in the FK-triangulation by Lemma 24, and Theorem 25.
 909 Conversely, suppose that (v'_0, ω') is the canonical permutahedral representation of a simplex
 910 in the star of v_0 , that is there is some k such that $v'_k = v_0$, with v'_k as in (3). Then
 911 $(v_0, \omega) = (v'_0, \omega') \oplus k$ is also a permutahedral representation of the same simplex. ◀

912 **Faces.** From (6) it is clear that merging two consecutive parts in the ordered partition
 913 $\omega = (\omega_1, \dots, \omega_{l+1})$ corresponds to removing a vertex from the simplex, that is taking a facet.
 914 Here we stress that we allow to merge ω_1 , and ω_{l+1} , but in that case we have to change
 915 the base point of the cycle to $v_0 + \sum_{l \in \omega_1} e_l$ to obtain the canonical representation. For
 916 example, when looking at the two dimensional example in Figure 1, we see that the edges
 917 that contain y in the red triangle with permutahedral representation $(y, (\{1\}, \{2\}, \{3\}))$ are
 918 $(y, (\{1, 2\}, \{3\}))$, and $(y, (\{1\}, \{2, 3\}))$. The third edge of the red triangle is $(y', (\{2\}, \{1, 3\}))$.
 919 Generally, given an ordered partition ω in $l + 1$ parts all $(l - j)$ -faces can be found by merging
 920 j consecutive parts in ω (for example merging ω_1 with ω_2 , and ω_3 with ω_4), where we allow
 921 ω_{l+1} to merge with ω_1 , but in this case we again need to change the base point to obtain the
 922 canonical representation.

923 Because the combinatorial structure of the faces is compatible with the permutahedron,
 924 Lemma 32 immediately gives the following result. We recall that two complexes are dual if
 925 there is a bijection between the faces that inverses the inclusion relationships (see for example
 926 [14, Section 11.3]).

927 ► **Proposition 33.** *The star of a vertex in a CFK-triangulation is combinatorially dual to a*
 928 *permutahedron.*

929 This proposition explains the nomenclature permutahedral representation.

930 This is equivalent to the following more geometric result:

931 ► **Proposition 34.** *The Voronoi cell of a Coxeter triangulation of type \tilde{A}_d is a permutahedron.*

932 This can be found in [21, Chapter 21, Section 3.F], see also [19]. We note that Coxeter
 933 triangulations of type \tilde{A}_d are combinatorially equivalent to FK-triangulations as discussed
 934 below in Section A.1.3. In the appendix we give a new proof that is more direct than the
 935 one in [21].

936 **Duality.** We can associate to a FK-triangulation \mathcal{T} its dual complex \mathcal{T}^* . Since \mathcal{T} is a
 937 simplicial complex, \mathcal{T}^* is a simple complex, that is a cell complex whose faces are all simple
 938 polytopes [14]. By Proposition 33, each d -dimensional cell of \mathcal{T}^* is a d -permutahedron.

939 A.2.2 Basic operations on FK-triangulations

940 **Point location.** Given a point $x \in \mathbb{R}^d$ Lemma 24 tells us how to find the canonical
 941 permutahedral representation of the simplex in which x is contained. The complexity of
 942 point location is dominated by the sorting of the $z^i = x^i - \lfloor x^i \rfloor$, which takes $O(d \log d)$ time,
 943 and requires $O(d)$ space.

944 **Face computation.** Let σ be an l -simplex whose canonical permutahedral representation is
 945 (v_0, ω) , where ω is an ordered partition of $[d + 1]$ into $l + 1$ parts. The computation of all
 946 k -faces of σ goes as follows. We use Ehrlich's subset generation algorithm [27] to compute
 947 all the subsets of $k + 1$ elements from $\{v_0, \dots, v_l\}$. Let $\tau = \{v_{m_0}, \dots, v_{m_k}\}$ be such a subset.
 948 τ is a k -face of σ . We then compute the canonical permutahedral representation of all those
 949 k -faces τ .

950 We first sort the m_i so that $m_0 < \dots < m_k$ using counting sort. Then, the canonical
 951 permutahedral representation (\tilde{v}'_0, ω') of τ is found by merging consecutive parts of ω so as
 952 to obtain $k + 1$ parts as follows :

$$953 \quad v'_0 = v_{m_0} = v_0 + \sum_{j \in \omega_1} e_j + \dots + \sum_{j \in \omega_{m_0-1}} e_j$$

$$954 \quad \omega'_i = \omega_{m_{i-1}} \cup \dots \cup \omega_{m_i-1} \quad \text{for } i \in \{1, \dots, k\}$$

$$955 \quad \omega'_{k+1} = (\omega_1 \cup \dots \cup \omega_{m_0-1}) \cup (\omega_{m_k} \cup \dots \cup \omega_{l+1}).$$

956 The complexity of computing all subsets of $k + 1$ vertices of σ using Ehrlich's algorithm
 957 takes time $O(k + s)$ where $s = \binom{l+1}{k+1}$ is the number of subsets. Computing, for each such
 958 k -simplex its permutahedral representation takes $O(d)$ time.

959 ► **Lemma 35 (Face computation (full version)).** *Let σ be an l -simplex in the FK-triangulation
 960 of \mathbb{R}^d given by its canonical permutahedral representation. Computing the canonical permutahedral
 961 representations of all its k -faces can be done in time $O(ds)$, where $s = \binom{l+1}{k+1}$ is the
 962 number of k -faces of an l simplex. The space complexity of the algorithm is $O(l)$.*

963 **Coface computation.** Computing the faces of a simplex σ consists in coarsifying its ordered
 964 partition. The computation of cofaces is the reverse. Here we refine the ordered partition.
 965 Specifically, if σ is a k -simplex represented by its canonical permutahedral representation
 966 (v_0, ω) , and we want to compute its l -cofaces, we need to compute all refinements of ω into
 967 $l + 1$ parts.

968 More precisely, we need to subdivide each ω_i in $a_i \leq |\omega_i|$ subparts so that $\sum_{i=1}^{k+1} a_i = l + 1$.
 969 This can be done in time proportional to the number $k + 1$ of the generated subparts. We
 970 then need to consider all the permutations of these subparts since we are interested in ordered

971 partitions. Using known algorithms by Walsh [43], and Ruskey and Savage [40], we can
 972 compute all the ordered partitions associated to the l -cofaces of σ in time proportional to
 973 the number of such cofaces. We thus obtain all the permutahedral representations (v_0, ω') of
 974 all the l -cofaces of σ .

975 It is important to notice that all cofaces of σ have v_0 as a vertex. However v_0 is not necessarily
 976 the minimal vertex of some of the computed cofaces. We thus have to identify the minimal
 977 vertex of each computed coface, and use cyclic shifts (as in Lemma 32) to obtain the canonical
 978 permutahedral representation of the coface. The next Lemma follows. The bound on the
 979 number s of cofaces follows, by duality, from Corollary 22.

980 ► **Lemma 36** (Coface computation (full version)). *Let σ be a k -simplex in the FK-triangulation*
 981 *of \mathbb{R}^d given by its permutahedral representation. Computing the permutahedral representations*
 982 *of all its l -cofaces can be done in time $O(ds)$, where*

$$983 \quad s = p_{d-l, d-k} \leq \frac{1}{2^{\min(l, d-l)}} \binom{d-k}{d-l} (d-k+1)!$$

984 *is the number of l -cofaces of a k -simplex in the FK-triangulation. The space complexity of*
 985 *the algorithm is $O(d)$.*

986 A.3 Data structure for CFK-triangulations

987 We store a CFK-triangulation as follows. The combinatorial structure of the triangulation is
 988 given through the canonical permutahedral representation of its simplices, and the algorithms
 989 from Section A.1.2. The geometry of the triangulation is specified by the affine transformation
 990 that maps the FK-triangulation of \mathbb{R}^d to the CFK-triangulation. The affine transformation
 991 is given by a $d \times d$ matrix Λ , and a d -vector b . For the FK-triangulation, Λ is the identity
 992 matrix, and $b = 0$; therefore no storage is required. For the Coxeter triangulation of type \tilde{A}_d ,
 993 Λ is sparse, as can be seen by inspection of the proof of Lemma 28.

994 A.4 Experimental results for the datastructure

995 The data structure and the basic operations have been implemented in C++ and are currently
 996 under review to be integrated in the GUDHI library. We report on the execution time of the
 997 face and coface generation algorithms for the FK-triangulations.

998 In Tables 1-4, we consider an ambient space of moderate dimension $d = 30$ and compute the
 999 higher dimensional faces of various high dimensional simplices, of dimensions ranging from
 1000 22 to 30.

1001 Each entry in Table 1 corresponds to the total time in milliseconds of computing all the
 1002 k -dimensional faces of a set of l -dimensional simplices in \mathbb{R}^{30} . The l -dimensional simplices
 1003 are picked at random in the triangulation and the results are averaged over 1 000 simplices.
 1004 Note that the time 11 904.7ms is the time of computing all 5 852 925 faces of dimension 22 of
 1005 a simplex of dimension 30.

1006 Table 2 shows the same running times per computed face. As we can see, except for the case
 1007 $l = k$, the running time per computed face is around $2\mu s$.

XX:32 Isomanifold Tracing in \mathbb{R}^d , using Coxeter-Freudenthal-Kuhn Triangulations

Face dimension k		22	23	24	25	26	27	28	29	
1008	Simplex dimension l	22	0.006							
1009		23	0.042	0.006						
1010		24	0.503	0.05	0.008					
1011		25	4.88	0.645	0.058	0.008				
1012		26	33.76	5.697	0.697	0.062	0.008			
1013		27	162.114	35.108	6.824	0.758	0.064	0.008		
1014		28	885.293	190.441	40.856	6.906	0.739	0.058	0.006	
1015		29	3420.99	973.455	246.88	49.896	6.657	0.735	0.058	0.006
1016		30	11904.7	4175.92	1247.97	275.776	50.932	7.348	0.778	0.058

1017 **Table 1** Total running time of the face generation algorithm (in milliseconds).

Face dimension k		22	23	24	25	26	27	28	29	
1018	Simplex dimension l	22	0.006							
1019		23	0.0018	0.006						
1020		24	0.0017	0.002	0.008					
1021		25	0.0019	0.002	0.0022	0.008				
1022		26	0.0019	0.0019	0.002	0.0023	0.008			
1023		27	0.0016	0.0017	0.0021	0.002	0.0023	0.006		
1024		28	0.0019	0.0016	0.0017	0.0019	0.0018	0.002	0.006	
1025		29	0.0017	0.0016	0.0017	0.0018	0.0016	0.0017	0.0019	0.006
1026		30	0.0015	0.0016	0.0017	0.0016	0.0016	0.0016	0.0017	0.0019

1027 **Table 2** Running time of the *face* generation algorithm *per computed face* (in milliseconds).

1028 In Tables 3 and 4, we present analogous tables for the coface computation algorithm. Similarly,
 1029 the running time per computed coface in Table 4 is around $2\mu s$ with the exception of when
 1030 k is close to l .

Coface dimension l		23	24	25	26	27	28	29	30
Simplex dimension k	22	0.11	1.274	9.577	43.848	86.699	96.407	59.935	15.487
	23	0.043	0.114	0.729	3.499	9.337	13.523	10.058	3.049
	24		0.047	0.1	0.381	1.183	2.132	1.871	0.653
	25			0.046	0.097	0.23	0.423	0.426	0.193
	26				0.047	0.076	0.128	0.15	0.093
	27					0.049	0.069	0.081	0.063
	28						0.047	0.061	0.054
	29							0.05	0.053
	30								0.05

1040 ■ **Table 3** Total running time of the *coface* generation algorithm (in milliseconds).

Coface dimension l		23	24	25	26	27	28	29	30
Simplex dimension k	22	0.002	0.0013	0.0013	0.0015	0.0016	0.0016	0.0016	0.0017
	23	0.042	0.003	0.0017	0.0016	0.0016	0.0016	0.0016	0.0017
	24		0.045	0.004	0.0019	0.0017	0.0017	0.0017	0.0018
	25			0.045	0.0053	0.0025	0.002	0.0019	0.0022
	26				0.047	0.0073	0.0035	0.0028	0.0036
	27					0.048	0.0103	0.0058	0.0068
	28						0.048	0.0145	0.0133
	29							0.05	0.026
	30								0.05

1050 ■ **Table 4** Running time of the *coface* generation algorithm *per computed face* (in milliseconds).

XX:34 Isomanifold Tracing in \mathbb{R}^d , using Coxeter-Freudenthal-Kuhn Triangulations

1051 The next results are motivated by the problem of tracing a manifold of low dimension m
 1052 embedded in \mathbb{R}^d for high d . The crucial operations in this context consist in computing the
 1053 facets and cofacets of simplices of codimension m in a triangulation of \mathbb{R}^d , as is clear from
 1054 Algorithm 1 .

1055 In Table 5, we present the execution time of the *facet* generation algorithm applied to
 1056 simplices of low codimension m , ranging from 1 to 7, in FK-triangulations of high dimensions
 1057 d (up to $d = 400$). In Table 6, we present the execution time of the *cofacet* generation
 1058 algorithm under the same circumstances.

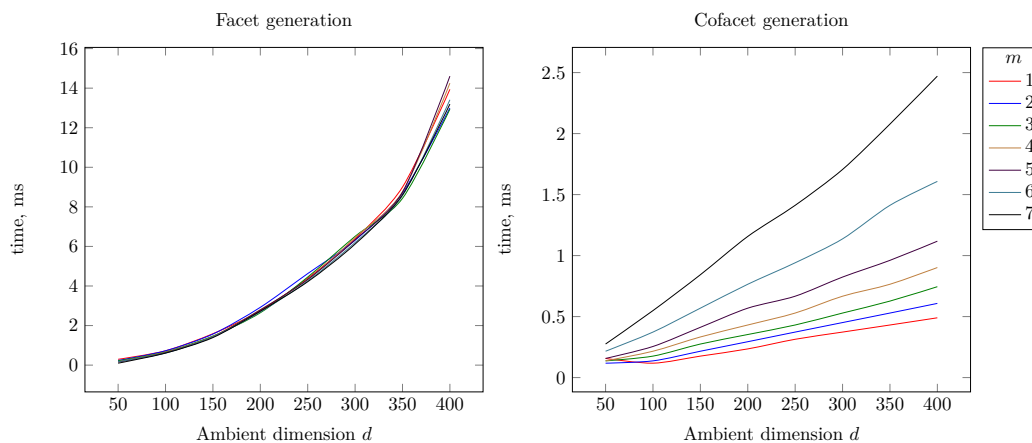
Ambient dimension d	50	100	150	200	250	300	350	400	
Face codimension m	1	0.166	0.612	1.438	2.862	5.376	8.69	12.184	15.924
	2	0.166	0.643	1.417	2.858	5.607	8.375	11.806	16.261
	3	0.168	0.607	1.395	2.888	5.866	8.232	12.008	16.527
	4	0.162	0.589	1.373	2.864	5.491	8.447	11.936	16.08
	5	0.154	0.587	1.349	2.76	5.77	8.371	11.814	15.88
	6	0.148	0.579	1.321	2.737	5.735	8.351	12.038	15.798
	7	0.136	0.575	1.313	2.553	5.701	8.313	12.11	15.754

1066 ■ **Table 5** Average running times in milliseconds of the *facet* generation algorithm.

Ambient dimension d	50	100	150	200	250	300	350	400	
Simplex codimension m	1	0.068	0.134	0.228	0.281	0.423	0.605	0.611	0.848
	2	0.082	0.17	0.267	0.341	0.483	0.723	0.731	0.966
	3	0.098	0.194	0.303	0.401	0.525	0.733	0.866	1.124
	4	0.112	0.226	0.351	0.467	0.665	0.806	0.974	1.295
	5	0.132	0.265	0.423	0.545	0.966	0.928	1.128	1.477
	6	0.162	0.329	0.515	0.713	0.948	1.124	1.361	1.76
	7	0.2	0.415	0.651	0.878	1.166	1.421	1.784	2.283

1074 ■ **Table 6** Average running times in milliseconds of the *cofacet* generation algorithm.

1075 A graphical display of the results of Tables 5 and 6 is shown in Figure 10.



1076 ■ **Figure 10** Graphical display of the results of Tables 5 and 6.

1077 **B Proofs**

1078 **Proof of Proposition 9.** The complexity of the initialization is $O(d)$. The complexity of each
 1079 iteration of the while loop consists of computing the cofacets of the popped k -dimensional
 1080 simplex in the queue, computing facets of these cofacets, and applying the intersection oracle
 1081 on each of these facets. An upper bound on the number of cofacets of a k -simplex in a
 1082 CFK-triangulation follows, by duality, from Corollary 21, specifically $O(2^n)$. Each of these
 1083 cofacets has $k + 2$ facets. Therefore, for each iteration of the while loop, the algorithm applies
 1084 the intersection oracle on $O(k2^n)$ simplices. By using this observation, and the complexities
 1085 in Lemmas 35, and 36, the total time complexity of each iteration of the while loop follows:

1086
$$O(d2^n) + O(dk2^n) + O(k2^n I) = O(k2^n(d + I)) = O(k2^n I).$$

1087 Since there are $|\mathcal{S}|$ iterations of the while loop, the result follows. ◀

1088 **Proof of Proposition 10.** By the definition of CFK-triangulations in Section A.1, \mathcal{T} is an
 1089 arrangement of $d(d - 1)/2$ families H_u of hyperplanes, $u \in E_{\mathcal{T}}$. Each family H_u consists of
 1090 the hyperplanes $H_{u,k}, k \in \mathbb{Z}$, all orthogonal to u . Let $L_{\mathcal{T}}$ be the length of the longest edge
 1091 of a simplex in \mathcal{T} and $R_{\mathcal{T}}$ be the maximal norm of the vectors u . Note that the distance
 1092 between two consecutive hyperplanes in family H_u is $1/\|u\| \geq 1/R_{\mathcal{T}}$.

1093 We will rescale the arrangement of hyperplanes so that the maximal diameter of the simplices
 1094 is D , the required precision. Hence the distance between two consecutive hyperplanes in
 1095 H_u is $D/(L_{\mathcal{T}}\|u\|)$. It follows that at most $\sqrt{d}L_{\mathcal{T}}\|u\|/D$ hyperplanes of family H_u intersect
 1096 the unit cube C_d that contains \mathcal{M} (which has diameter \sqrt{d}). Consider any subset of n
 1097 families among the $d(d - 1)/2$ families, and write I for the associated subset of indices,
 1098 $I \subset [1, d(d - 1)/2], |I| = n$. Now take n hyperplanes, one in each family $H_{u_i}, i \in I$. Their
 1099 common intersection is an affine space of dimension $k = d - n$. This affine space intersects \mathcal{M}
 1100 in at most K points under the general position assumption and the fact that \mathcal{M} is K -sparse.
 1101 The total number of intersection points $N_{\mathcal{T}} = \mathcal{T}_k \cap \mathcal{M}$ is thus bounded as follows

1102
$$N_{\mathcal{T}} \leq K \binom{d(d - 1)/2}{n} \times \prod_{i \in I} \frac{\sqrt{d}L_{\mathcal{T}}\|u_i\|}{D} \leq \frac{K}{n!} \times \left(\frac{d^2 \sqrt{d}L_{\mathcal{T}}R_{\mathcal{T}}}{2D} \right)^n. \tag{8}$$

1103 Here the binomial coefficient arises as the number of choices of n families of hyperplanes.
 1104 Consider now more specifically Coxeter triangulations of type \tilde{A}_d and FK -triangulations. It
 1105 follows from Section A.1 that $R_C = R_{FK} = \sqrt{2}$. The longest edge L_{FK} in a Freudenthal-
 1106 Kuhn triangulation has length at most (in fact exactly) \sqrt{d} since each simplex is contained
 1107 in a cubical cell of the d -dimensional unit grid. Furthermore, it is proved in [18, point 6 of
 1108 \tilde{A}_d in Section 6] that the longest edge length in the Coxeter triangulation of type \tilde{A}_d is

1109
$$L_C = \begin{cases} \frac{\sqrt{d+1}}{2} & \text{if } d \text{ is odd,} \\ \frac{1}{2} \sqrt{\frac{d(d+2)}{d+1}} & \text{if } d \text{ is even,} \end{cases} \tag{9}$$

1110 and hence $L_C < \frac{\sqrt{d+2}}{2}$. We then deduce from (8)

1111
$$N_C \leq \frac{K}{n!} \times \left(\frac{d^2 \sqrt{d(d+2)}}{2\sqrt{2}D} \right)^n$$

1112
$$N_{FK} \leq \frac{K}{n!} \times \left(\frac{d^3}{\sqrt{2}D} \right)^n.$$

1113 ◀

1114 **Proof of Proposition 11.** Let σ be a k -simplex of a CFK-triangulation that intersects $\hat{\mathcal{M}}$,
 1115 and let σ^* be its dual cell. By definition, σ^* is a m -dimensional face of \mathcal{T}^* , the polytopal cell
 1116 complex dual to \mathcal{T} . The collection of all σ^* associated to the k -simplices σ of \mathcal{T} that intersect
 1117 $\hat{\mathcal{M}}$ form a cell complex $\hat{\mathcal{M}}^*$ dual to $\hat{\mathcal{M}}$. To bound the number of faces of all dimensions of
 1118 the PL-approximation $\hat{\mathcal{M}}$, it is therefore sufficient to bound the number of faces of $\hat{\mathcal{M}}^*$.
 1119 Each d -dimensional cell in \mathcal{T}^* is a permutahedron (Proposition 33). Hence, σ^* is a n -face of
 1120 a d -permutahedron. The number of faces of σ^* of dimensions 0 to $n - 1$ (or equivalently
 1121 the number of cofaces of σ of dimensions $n + 1$ to d) is:

$$1122 \quad \sum_{i=0}^{n-1} p_{i,n} \leq \sum_{i=0}^{n-1} \frac{1}{2^i} \binom{n}{i} (n+1)! = \frac{3^n - 1}{2^n} (n+1)!$$

1123 where $p_{i,j}$ denotes the number of i -faces of a j -face of the d -permutahedron and is bounded
 1124 in Corollary 22. The last equality can be easily verified using Mathematica. The overall
 1125 combinatorial complexity of $\hat{\mathcal{M}}$ is therefore

$$1126 \quad |\mathcal{S}| \times \frac{3^n - 1}{2^n} (n+1)!,$$

1127 where \mathcal{S} is bounded in Proposition 10. ◀

1128 **C** Alternative Proof of Proposition 34

1129 **Proof of Proposition 34.** We start by recalling a number of results. Let $P = \{(x^i) \in \mathbb{R}^{d+1} \mid$
 1130 $\sum_i x^i = 0\}$ and consider the d -simplex with vertices u_k in P .

$$1131 \quad u_0 = \left(0^{\{d+1\}}\right) \quad u_k = \left(\left(-\frac{d+1-k}{d+1}\right)^{\{k\}}, \left(\frac{k}{d+1}\right)^{\{d+1-k\}} \right), \quad k \in [d],$$

1132 where $x^{\{k\}}$ denotes k consecutive coordinates x . This simplex is a simplex in the Coxeter
 1133 triangulation, as defined in Section A.1.3. In [18] we have seen that the circumcentre of this
 1134 simplex is

$$1135 \quad c = \left(-\frac{d-2i}{2(d+1)}\right),$$

1136 with $i \in \{0, \dots, d\}$. The circumcentre of a Delaunay simplex is a Voronoi vertex. We recall
 1137 that

- 1138 ■ All simplices in the star of 0 in the Coxeter triangulation are found by consecutive
 1139 reflection of a single simplex (in this star) in the hyperplanes of \mathcal{H}_{EC} that go through
 1140 0, that is the hyperplanes with normals $r_{j,k} = e_j - e_k$, with $j \neq k$. See for example
 1141 [15, 31, 18]. We also call these reflections the action of the Weyl group.
- 1142 ■ The reflection $R_{j,k}$ in a plane that goes through the origin with normal $r_{j,k}$ is given by

$$1143 \quad R_{j,k}(v) = v - 2 \frac{v \cdot r_{j,k}}{r_{j,k} \cdot r_{j,k}} r_{j,k} = v - (v \cdot r_{j,k}) r_{j,k}.$$

1144 We find that

$$1145 \quad R_{j,k}(c)^i = (c - (c \cdot r_{j,k}) r_{j,k})^i = -\frac{d-2i}{2(d+1)} - \frac{2j-2k}{2(d+1)} (\delta_{ij} - \delta_{ik}),$$

1146 which permutes the j th and k th coordinate of c . Here we used the upper index i to denote
 1147 the i th coordinate. Using the cycle notation for the permutation group, see for example [5,
 1148 Chapter 6], this coincides the 2-cycle $(j\ k)$. Let now

$$1149 \quad c_\pi = \left(-\frac{d - 2\pi_i}{2(d+1)} \right),$$

1150 with $\{\pi_i\}$ some permutation of $\{0, \dots, d\}$. We find that

$$1151 \quad R_{j,k}(c_\pi)^i = (c_\pi - (c_\pi \cdot r_{j,k})r_{j,k})^i = -\frac{d - 2\pi_i}{2(d+1)} - \frac{2\pi_j - 2\pi_k}{2(d+1)}(\delta_{ij} - \delta_{ik}),$$

1152 which again permutes the j th and k th coordinate. Now recall that all permutations are
 1153 generated by 2-cycles, see for example [5, Theorem 6.1]. This implies that, for any permutation
 1154 π , we can find c_π from c by the action of the Weyl group. This also means that we have
 1155 explicitly described the Voronoi cell of 0 in the Coxeter triangulation of type \tilde{A}_d as a
 1156 permutahedron. Because of symmetry, this now holds for any Voronoi cell. ◀